NMR Studies on Structure and Dynamics of Ribosome Recycling Factor

Takuya Yoshida

NMR Studies on Structure and Dynamics of Ribosome Recycling Factor

A Doctoral Thesis

Submitted to the Graduate School of Pharmaceutical Sciences

Osaka University

Takuya Yoshida

2003

Contents

General Introduction

Chapter I

NMR Assignments of Ribosome Recycling Factors

Chapter II

Solution Structure of the Ribosome Recycling Factor from *Aquifex aeolicus*

Chapter III

A Characteristic Domain Motion in the Ribosome Recycling Factor Revealed by ^{15}N NMR Relaxation Experiments and Molecular Dynamics Simulations

Concluding Remarks

References

Acknowledgements

General Introduction

In protein biosynthesis, the sequence of codons on mRNA is translated to a polypeptide chain. This process takes place on the ribosome, which is a large ribonucleoprotein particle, consists of two subunits. In eubacteria, the subunits are designated 30S and 50S, and together compose the 70S ribosome. As shown in Figure 0-1, protein biosynthesis on the ribosome consists of four steps: initiation, peptide chain elongation, termination, and ribosome recycling.

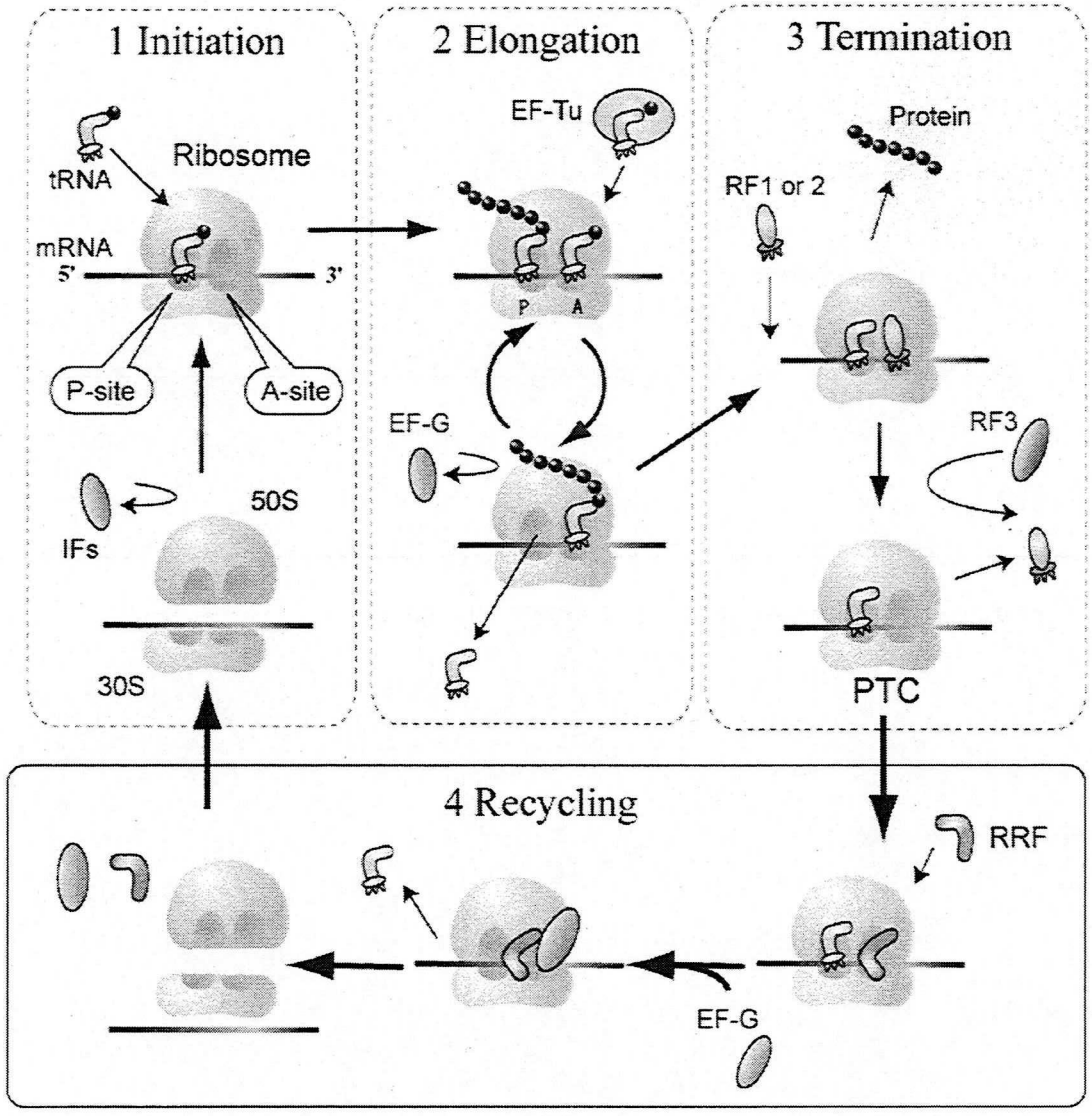

Figure 0-1. Four steps of protein biosynthesis in eubacteria. (The E-site, to which discharged tRNAs are transferred before being rereased, is not shown.)

At the termination step, RF1 or RF2 (release factor 1 or 2) recognizes the stop codon on mRNA and then promotes the hydrolysis of peptidyl-tRNA at the P-site of the ribosome to release the nascent peptide chain. After the hydrolysis of peptidyl tRNA, followed by release of RF1 or RF2 from A site of ribosome by the action of RF3, the so-called post-termination complex (PTC), composed of 70S ribosome, deacylated tRNA, and mRNA, remains. The resulting PTC must be recycled for the next round of protein biosynthesis. In 1970, Kaji and his coworkers found a protein that catalyzes the breakdown of PTC into 70S ribosomes, tRNA and mRNA. They named it as the ribosome recycling factor (RRF) (*1*). (First it was called ribosome releasing factor but, it was renamed as ribosome recycling factor to avoid confusion with peptide release factor, RFs (*2*).) To examine the activity of RRF, they developed an assay method in vitro using a model PTC system prepared from puromycin-treated polysome. Each ribosome on the polysome has two deacylated tRNAs at the P and E sites and mRNA bound to it. This configuration is nearly identical to the natural PTC, except that the A site is not occupied with the termination codon. Treatment of this system with RRF and elongation factor G (EF-G) results in conversion of the polysome to monosomes, which is easily observed as a change in sedimentation profile. It has also been shown that, in the absence of RRF, ribosomes reinitiate to translate the 3' portion of the mRNA downstream from the termination codon (*3, 4*). Furthermore, RRF might has a role in maintainig translational fidelity during peptide chain elongation (*5*).

In vitro studies on the mechanism of the RRF action was performed using a synthetic polynucleotide with poly-A tail and strong Shine Dalgarno (SD) sequence close by the termination codon (*6-8*). It was found in this system that 50S subunit is dissociated from the 70S ribosome complex during the disassembly process. The remaining complex of tRNA, mRNA, and 30S subunit is separated by IF3. In contrast, with natural mRNA (*9, 10*), or with synthetic mRNA without the SD sequence (*11*), no ribosome remained on the mRNA. This indicates that the behavior of ribosomes in response to the action of RRF is very much dependent on the sequence of the mRNA surrounding the termination codon as demonstrated in vivo recently (*12*).

The assay system to examine the activity of RRF in vivo using a temperature sensitive mutant of RRF, e.g. V117D, has been established (*4*). In the temperature sensitive mutant cells, RRF is inactivated above 42°C. It was found that in vivo inactivation of RRF resulted in a bactericidal effect during the lag phase. The *frr* gene encoding RRF exists in most

organisms, except for in archaebacteria. Even in the smallest free-living organism such as *Mycoplasma genitalium* with only 500 genes an *frr* homolog was found (*13*). These facts strongly indicate that RRF is an essential protein for prokaryotes. On the other hand, it was found that RRF homolog in eukaryotes does not exist in cytoplasm. They might be localized and perform their functions only in organelles such as mitochondria and chloroplasts (*14*). Therefore, a compound which has an inhibitory activity on RRF should be an antimicrobial agent with novel type of antibiotic mechanism.

In addition of many genetic and biochemical studies as mentioned above, the crystal structures of RRFs were reported (*15-17*). These studies indicated that the structure of RRF is very similar to that of tRNA in shape and dimensions. Based on such similarity, a concept of molecular mimicry was proposed. Originally, it was suggested that domains I and II of RRF correspond to the anticodon and acceptor arms of tRNA, respectively (*15*). Thus it was proposed as a hypothetical mechanism that RRF would be bound first to the A-site of the ribosome and then translocated by EF-G to the P-site in a manner similar to that of tRNA, leading to the disassembly of the post-termination complex (*15*). The interaction between RRF and A-site is supported by the finding that RRF and RF1 have overlapping binding sites on the ribosome (*7*).

Although the model in which RRF acts as a mimic of tRNA is very attractive, no direct evidence for that hypothesis has been reported and the mechanism for disassembly of post-termination complex is not well understood. To better understand the activity of RRF, therefore, it is necessary to clarify that the interactions of RRF with ribosome or other factors and the physico-chemical property, structure, dynamics, stability etc. of RRF molecule in detail. The spatial arrangement of RRF in the RRF-ribosome complex was studied by several researchers so far. Hydroxyl radical probing of RRF binding site on ribosome demonstrated that the orientation of RRF in the ribosome differs from A-site bound tRNA (*18*). The author and colleagues revealed that domain I of RRF mainly acts as a 50S binding domain (*19*) by using an engineered domain I peptide and proposed a possible RRF-ribosome complex model where domain I was superimposed on the acceptor arm of tRNA.

In this study, the author have characterized RRFs of several bacteria by NMR spectroscopy in solution to better understand the function of RRF. In Chapter 1, the author will report the backbone ^{1}H, ^{13}C, and ^{15}N NMR assignments and the secondary structures of RRFs from *Pseudomonas aeruginosa*, *Escherichia coli*, *Aquifex aeolicus*, *Thermus thermophilus* and

Thermotoga maritima. In Chapter 2, the author will present the determination of the solution structure of *A. aeolicus* RRF by NMR. Resulting structure has a characteristic L-shaped conformation with two domains even in solution. In Chapter 3, the author will describe a domain motion in RRF molecule that was revealed by ^{15}N NMR relaxation experiments and molecular dynamics (MD) simulations.

Chapter I

NMR Assignments of Ribosome Recycling Factors

In the initial phase of any research using NMR spectroscopy, each nuclear magnetic resonance should be associated with a specific nucleus in the molecule under investigation. For peptides or small proteins with molecular mass of under 10 kDa, this phase, namely resonance assignment step, is based on sequential correlations obtained from homonucler 2D experiments via relatively small ^{1}H-^{1}H scalar coupling and ^{1}H-^{1}H NOE. On the other hand, for more larger proteins, resonance assignment should be performed using multinuclear multidimensional experiments, which are established via the relatively large heteronuclear one-bond and two-bond scalar couplings. For example, using HNCA and HN(CO)CA experiments together, the ^{1}HN and ^{15}N resonances are correlated with intraresidue and sequential $^{13}C\alpha$ resonances. In this chapter, the author presented resonance assignments of RRFs from several organisms. RRF consists of about 185 residues with molecular weight of 21 kDa. Thus, the author constructed bacterial expression system of RRF proteins in order to produce stable isotope labeled RRFs for multinuclear NMR experiments.

Experimental Procedures

Expression

The DNA fragments encoding RRF sequences from several bacteria were cloned into NdeI/BamHI sites of the pET22b plasmid vector (Novagen Madison, WI). The resulting recombinant RRF plasmids were pET-GRRF, pET-ERRF, pET-ARRF, pET-TTRRF, and pET-TMRRF for *Pseudomonas aeruginosa*, *Escherichia coli*, *Aquifex aeolicus*, *Theumus thermophilus*, and *Thermotoga maritima*, respectively. *E. coli* strain DH5α was used as a host strain for cloned plasmid DNA. *E. coli* strain BL21(DE3) was used for protein expression. Luria-Bertani (LB) broth (Nakalai tesque) was used in liquid media and solid agar media (1.5%) for routine cultivation of bacteria. Isotope labeled proteins were obtained from growing cells in isotope-enriched M9 minimal medium. The media were supplemented with 100 μg/ml ampicillin. The cells were grown at 37°C in M9 medium to A600=0.5 and the protein expression was induced by adding isopropyl-1-thio-β-D-galactopyranoside (IPTG) to

a final concentration of 1.0 mM, followed by 4h incubation. The bacteria were harvested by centrifugation. Harvested cells were suspended in buffer (50mM Tris-HCl pH 8.0, 50mM NaCl, 1mM EDTA, 1mM (4-amidinophenyl)-methanesulfonyl fluoridehydrochloride monohydrate (APMSF)) and disrupted by sonication. The homogenate was centrifuged to remove the insoluble debris. In the cases of *A. aeolicus* RRF, *T. thermophilus* RRF and *T. maritima* RRF, the supernatants were heated at 60-80 °C for 10 minutes and centrifuged. The heat treatment step simplified the purification procedure and decreased the protein loss because the majority of contaminating cellular proteins were denatured and precipitated. RRF was isolated and purified from the supernatant using DEAE-sepharose column and Superdex 75pg column. All RRFs were purified to homogeneity as judged by SDS-PAGE.

P. aeruginosa RRF

Uniformly labeled samples, [U-^{15}N], [U-^{15}N/^{13}C], and [U-^{2}H/^{15}N/^{13}C] *P. aeruginosa* RRF, were prepared for sequential assignments of backbone nuclei. Moreover selective ^{15}N labeling was performed for the following seven amino acids: Lys, Val, Met, Ile, Leu, His and Arg, according to the method described by Lee et al. (*20*). For the selective incorporation of Met and His residues, auxotrophic strains of *E. coli* for the corresponding amino acids were used. No isotopic dilution or incorporation of label at undesired sites was detected. The final NMR sample contained RRF at a concentration of ca. 1.5 mM in 10 mM potassium acetate buffer of 90% H_2O/10% D_2O at pH 5.0 with 50 mM NH_4Cl, 10 mM $MgSO_4$ and 1 M glycine.

All NMR spectra were acquired at 25 °C on a Varian INOVA600 or INOVA500 spectrometers with a tripleresonance z-gradient probehead. Pulsed-field gradient technique with a WATERGATE (*21*) or a Rance-Kay method (*22*) was used for all H_2O experiments. Transmitter frequencies for ^{1}H, ^{15}N, ^{13}Cα, aliphatic ^{13}C, aromatic ^{13}C, and carbonyl ^{13}C were typically 4.76, 119.0, 55.0, 43.0, 125.0 and 176 ppm, respectively. Proton chemical shifts were referenced with sodium 4,4-dimethyl-4-silapentane-1-sulfonate (DSS). ^{15}N and ^{13}C chemical shifts were indirectly referenced according to gyromagnetic ratio (*23*). The NMR experiments performed included sensitivity-enhanced 2D ^{1}H-^{15}N HSQC, 3D HNCA, HN(CO)CA, HA(CA)NH, HA(CACO)NH, HN(CA)CO, HNCO and 4D ^{15}N/^{15}N-NOESY. Other experimental details, together with the original references, are provided in the review (*24, 25*). Processing of the data was carried out using the NmrPipe software package (*26*). For analysis of the multidimensional spectra, PIPP/CAPP/STAPP (*27*) and in-house written

programs were used. The sequential resonance assignments were established by the combined analysis of the double- and triple-resonance NMR data of uniformly labeled RRF. The assignments were also facilitated and confirmed by seven selective ^{15}N-labeling experiments.

A. aeolicus RRF

The NMR samples of [U-^{15}N], [U-$^{15}N/^{13}C$], and [U-$^{2}H/^{15}N/^{13}C$] *A. aeolicus* RRF were prepared in 93% H_2O / 7% D_2O or 99.9% D_2O sodium acetate buffer of 20 mM at pH 5.2 with 20 mM NaCl. The protein solutions of 0.5 mM were used for NMR measurements. ^{15}N-^{1}H-HSQC, HNCO, HNCA, CBCANH, CBCA(CO)NH, and HN(CA)CO spectra were acquired at 40 °C.

E. coli RRF

The NMR samples of [U-^{15}N], [U-$^{15}N/^{13}C$], and [U-$^{2}H/^{13}C/^{15}N$] *E. coli* RRF were prepared in 90% H_2O/ 10% D_2O acetate buffer of 50mM at pH 5.0. The protein solutions of 0.5 mM were used for NMR measurements. ^{15}N-^{1}H-HSQC, HNCO, HNCA, CBCANH, CBCA(CO)NH, and HN(CA)CO spectra were acquired at 25 °C.

T. maritima RRF

The NMR sample of [U-$^{13}C/^{15}N$] *T. maritima* RRF was prepared in 90% H_2O/ 10% D_2O phosphate buffer of 50mM at pH 7.4. The protein solutions of 0.5 mM were used for NMR measurements. ^{15}N-^{1}H-HSQC, HNCO, HNCA, CBCANH, CBCA(CO)NH, and HN(CA)CO spectra were acquired at 40 °C.

T. thermophilus RRF

The NMR sample of [U-$^{13}C/^{15}N$] *T. thermophilus* RRF was prepared in 90% H_2O/ 10% D_2O HEPES buffer of 50mM at pH 7.4. The protein solutions of 0.5 mM were used for NMR measurements. ^{15}N-^{1}H-HSQC, HNCO, HNCA, CBCANH, CBCA(CO)NH, and HN(CA)CO spectra were acquired at 40 °C.

Results and Discussion

For five RRFs, almost all backbone ^{1}H, ^{15}N, and $^{13}C\alpha$ resonances were assigned successfully. For *P. aeruginosa* RRF, 171 out of 178 backbone amide resonances (185 residues minus six prolines and N-terminal) in the HSQC spectrum were unambiguously assigned. Those unassigned were Ile2, Gln10, Glu11, Thr114, Ser127, Thr164, and Phe167. For *A. aeolicus* RRF, complete assignments of backbone amide resonances, except for Leu5, were achieved. For *E. coli* RRF, complete assignments of backbone amide resonances, except for Ile2, were achieved. For *T. maritima* RRF, 164 out of 174 backbone resonances (185 residues minus 10 prolines and Met1) in the HSQC spectrum were unambiguously assigned. For *T. thermophilus* RRF, 170 out of 177 backbone resonances (185 residues minus 7 prolines and Met1) in the HSQC spectrum were unambiguously assigned. Unassigned resonances were not observed presumably due to conformational exchange or rapid exchange to solvent. The assigned chemical shift data (Table 1-1, 1-2, 1-3, 1-4 and 1-5) were deposited in BioMagResBank (http://www.bmrb.wisc.edu/). These data are essential for structural analyses and relaxation analyses to study dynamic properties of RRF molecule. Moreover, assignments of backbone amide resonances should be very useful for identifying interactions involving RRF and ribosomes, other transnational factors, and drugs.

The deviations of observed chemical shifts of α carbons from their standard values were calculated for five RRFs (Figire 1-1). It was widely accepted that such deviations are quite useful to assess the secondary structure of proteins (*28*). As shown in Figure 1-1, five α-helices and six β-strands are identified, of which three α-helices (α1, α3, α4) are characteristically long. No long loop nor unstructured region were indicated. These assignments of secondary structure elements were supported by NOE connectivity analysis for *P. aeruginosa* RRF. Although the origins of five RRFs are diverse, the profiles of secondary structures in solution are very similar among them. This fact suggests that overall structure of RRF is well conserved in eubacteria and essential for ribosome recycling activity. Thus, the author selected very stable RRF protein from a hyperthermophilic bacterium, *A. aeolicus*, as the target for solution structure determination in Chapter II.

Table 1-1. Chemical shift table of *A. aeolicus* RRF.

	aa	HN	N	Cα		aa	HN	N	Cα
1	MET	nd	nd	nd	51	LYS	8.46	122.35	55.07
2	ILE	8.79	121.87	61.55	52	VAL	9.09	123.69	58.21
3	LYS	8.71	127.69	59.30	53	PRO	nd	nd	nd
4	GLU	9.25	117.82	58.94	54	ILE	8.30	121.86	66.80
5	LEU	nd	nd	nd	55	LYS	8.22	114.07	58.19
6	GLU	8.32	117.94	59.27	56	GLN	7.93	117.76	56.12
7	ASP	8.35	119.33	57.73	57	LEU	7.92	117.33	53.82
8	ILE	7.45	121.55	65.37	58	GLY	6.80	106.52	45.73
9	PHE	7.79	117.71	63.41	59	THR	8.13	114.00	61.48
10	LYS	8.49	121.38	59.70	60	ILE	9.02	129.21	60.66
11	GLU	7.90	120.01	58.60	61	SER	9.41	121.90	56.96
12	ALA	8.49	120.77	54.49	62	VAL	8.41	119.31	nd
13	GLU	8.39	117.09	60.50	63	PRO	nd	nd	nd
14	LYS	7.65	119.14	60.10	64	GLU	7.34	114.28	53.95
15	ASP	8.17	120.18	57.24	65	HIS	8.86	116.38	58.31
16	MET	8.61	123.54	61.16	66	ASN	7.96	114.64	52.21
17	LYS	8.43	119.33	60.52	67	GLN	7.56	119.19	nd
18	LYS	8.00	119.26	59.42	68	ILE	8.57	120.25	59.75
19	ALA	7.57	122.08	55.29	69	VAL	9.04	126.94	60.99
20	VAL	8.00	119.68	67.23	70	ILE	9.34	126.82	59.70
21	GLU	8.52	121.29	59.76	71	GLN	8.71	127.77	54.50
22	TYR	8.42	120.39	61.16	72	VAL	8.74	125.95	62.86
23	TYR	8.03	121.03	60.96	73	TRP	7.76	126.76	58.92
24	LYS	8.83	118.96	60.27	74	ASP	9.07	120.13	51.88
25	ASN	7.77	117.25	56.00	75	GLN	9.04	125.93	58.77
26	GLU	8.15	121.07	59.47	76	ASN	8.60	115.93	55.52
27	ILE	8.22	112.34	64.22	77	ALA	8.34	120.22	52.71
28	ALA	7.40	124.63	54.22	78	VAL	7.32	116.93	69.14
29	GLY	7.33	128.45	44.97	79	PRO	nd	nd	nd
30	LEU	7.08	121.05	54.21	80	ALA	7.46	119.81	54.85
31	ARG	8.19	125.12	56.30	81	ILE	8.05	120.25	65.49
32	THR	8.25	113.58	60.50	82	GLU	8.62	120.17	61.00
33	SER	8.10	114.28	58.91	83	LYS	7.74	117.25	59.57
34	ARG	8.04	121.33	55.16	84	ALA	7.66	120.68	54.98
35	ALA	8.59	126.52	52.97	85	ILE	8.23	116.95	65.36
36	SER	6.97	112.15	56.72	86	ARG	8.06	120.37	60.01
37	THR	8.93	115.64	65.74	87	GLU	8.47	116.95	58.95
38	ALA	7.86	123.90	54.32	88	GLU	8.37	116.11	58.30
39	LEU	7.29	116.30	57.18	89	LEU	8.10	113.85	54.40
40	VAL	7.10	129.51	60.38	90	ASN	7.76	115.68	54.29
41	GLU	7.81	117.58	59.84	91	LEU	6.73	114.87	52.97
42	GLU	8.25	112.72	54.75	92	ASN	8.54	117.76	50.37
43	ILE	7.28	123.09	63.16	93	PRO	nd	nd	nd
44	LYS	8.36	125.55	55.03	94	THR	8.87	114.88	61.54
45	VAL	8.85	120.33	59.49	95	VAL	8.69	125.82	61.46
46	GLU	8.39	125.07	56.58	96	GLN	8.87	128.49	54.83
47	TYR	9.02	129.15	57.67	97	GLY	9.11	118.12	47.73
48	TYR	8.68	125.28	59.39	98	ASN	8.48	125.35	52.70
49	GLY	8.41	104.36	45.85	99	VAL	8.02	120.12	62.05
50	SER	7.70	115.89	56.87	100	ILE	9.10	127.84	59.80

Table 1-1. Continued.

	aa	HN	N	Cα		aa	HN	N	Cα
101	ARG	9.08	126.56	54.76	151	GLU	7.81	120.63	59.17
102	VAL	9.28	125.01	60.96	152	LYS	8.49	121.38	60.92
103	THR	8.43	123.73	61.31	153	LYS	8.25	118.97	60.37
104	LEU	8.86	128.93	52.29	154	ARG	7.98	119.04	59.43
105	PRO	nd	nd	nd	155	ALA	8.51	123.98	55.09
106	PRO	nd	nd	nd	156	LEU	8.71	119.86	58.20
107	LEU	8.54	122.27	54.80	157	GLU	7.97	122.40	59.54
108	THR	7.59	112.80	60.33	158	ARG	8.01	121.95	59.50
109	GLU	9.02	122.09	59.96	159	LEU	8.86	120.50	57.46
110	GLU	8.74	117.90	59.86	160	GLN	8.39	124.00	59.09
111	ARG	7.71	120.56	57.90	161	LYS	7.97	118.77	59.38
112	ARG	8.50	119.64	60.72	162	LEU	8.07	121.82	58.22
113	ARG	8.00	116.43	59.72	163	THR	7.94	114.86	67.26
114	GLU	7.86	120.52	59.15	164	ASP	8.54	120.39	57.47
115	LEU	8.46	120.58	58.07	165	LYS	7.79	120.98	59.49
116	VAL	8.24	119.45	67.36	166	TYR	7.64	118.60	64.11
117	ARG	7.85	120.98	60.27	167	ILE	8.71	121.61	63.84
118	LEU	8.23	122.05	58.05	168	ASP	8.41	119.08	57.40
119	LEU	8.86	119.54	58.04	169	GLU	7.68	119.19	60.19
120	HIS	8.98	121.68	59.29	170	ILE	7.84	120.00	66.00
121	LYS	8.13	123.85	60.28	171	ASN	8.62	118.95	55.97
122	ILE	8.81	118.88	65.03	172	LYS	8.52	121.60	59.52
123	THR	8.42	117.42	66.56	173	LEU	8.18	123.09	58.13
124	GLU	8.06	123.15	59.24	174	MET	9.09	121.91	nd
125	GLU	7.81	117.71	59.79	175	GLU	8.42	119.22	59.30
126	ALA	7.73	122.95	55.40	176	ALA	7.69	120.60	54.94
127	ARG	8.26	117.03	nd	177	LYS	8.09	120.78	56.51
128	VAL	8.52	119.55	66.87	178	GLU	9.22	122.20	61.04
129	ARG	7.78	119.44	60.25	179	LYS	7.72	117.22	59.58
130	VAL	7.86	119.72	68.02	180	GLU	7.65	120.06	59.46
131	ARG	8.70	119.36	60.50	181	ILE	8.27	119.72	65.58
132	ASN	8.86	122.01	55.85	182	MET	7.90	113.68	55.09
133	VAL	7.76	122.48	66.19	183	SER	7.58	115.02	59.22
134	ARG	7.69	119.34	60.20	184	VAL	7.74	125.78	64.13
135	ARG	8.08	119.13	59.98					
136	GLU	7.87	118.70	59.22					
137	ALA	8.36	122.02	54.83					
138	LYS	8.78	119.63	59.95					
139	GLU	7.60	117.50	58.98					
140	MET	7.56	116.60	59.00					
141	ILE	8.30	119.67	65.61					
142	GLU	8.29	116.31	59.34					
143	GLU	7.43	115.50	55.86					
144	LEU	7.23	122.04	56.04					
145	GLU	8.50	124.44	56.23					
146	GLY	8.67	108.66	46.01					
147	ILE	7.07	114.43	59.19					
148	SER	8.89	121.53	57.69					
149	GLU	8.99	121.49	59.73					
150	ASP	8.44	118.19	57.44					

Table 1-2. Chemical shift table of *E. coli* RRF.

	aa	HN	N	Cα		aa	HN	N	Cα
1	MET	nd	nd	nd	51	LEU	8.11	124.25	58.44
2	ILE	nd	nd	65.62	52	ARG	8.71	113.23	57.41
3	SER	8.55	114.96	60.72	53	GLN	7.78	115.39	56.36
4	ASP	7.41	120.92	56.64	54	LEU	7.80	116.89	53.84
5	ILE	7.51	122.28	64.19	55	ALA	7.51	122.28	50.09
6	ARG	8.25	120.76	59.52	56	SER	8.05	113.25	55.94
7	LYS	7.85	119.01	58.66	57	VAL	8.55	126.30	61.02
8	ASP	7.83	118.00	56.76	58	THR	9.14	118.52	59.18
9	ALA	8.20	120.36	54.47	59	VAL	8.66	121.50	62.18
10	GLU	8.34	118.63	59.54	60	GLU	8.58	130.02	56.92
11	VAL	8.17	119.08	65.62	61	ASP	8.39	116.07	53.06
12	ARG	8.46	119.07	59.90	62	SER	8.40	109.23	61.25
13	MET	9.03	119.81	61.25	63	ARG	8.37	117.96	55.03
14	ASP	8.26	119.94	57.42	64	THR	7.61	116.44	62.55
15	LYS	8.13	119.18	59.16	65	LEU	8.37	125.59	52.74
16	CYS	7.85	119.01	62.86	66	LYS	9.22	122.92	54.75
17	VAL	7.98	121.34	66.70	67	ILE	9.39	126.90	59.46
18	GLU	8.62	119.10	58.68	68	ASN	8.67	126.32	51.85
19	ALA	8.41	122.10	54.83	69	VAL	8.65	123.93	61.54
20	PHE	7.55	119.56	59.41	70	PHE	7.80	125.03	58.39
21	LYS	8.34	118.63	59.90	71	ASP	8.83	119.05	51.59
22	THR	8.66	117.26	66.22	72	ARG	8.89	124.71	58.76
23	GLN	8.11	122.86	59.20	73	SER	8.63	115.95	60.72
24	ILE	8.14	112.75	63.93	74	MET	8.31	118.63	53.63
25	SER	7.59	117.84	60.34	75	SER	7.72	115.76	64.10
26	LYS	7.07	118.13	55.96	76	PRO	nd	nd	65.87
27	ILE	7.14	119.89	59.97	77	ALA	7.57	119.77	54.53
28	ARG	8.48	129.13	55.37	78	VAL	8.23	120.22	66.35
29	THR	8.30	113.39	60.45	79	GLU	8.55	119.19	60.44
30	GLY	8.59	108.01	44.98	80	LYS	8.16	117.64	59.04
31	ARG	7.80	119.69	54.69	81	ALA	7.80	121.36	54.35
32	ALA	8.50	126.53	52.73	82	ILE	8.05	117.26	64.76
33	SER	7.11	114.90	54.36	83	MET	8.23	120.21	58.53
34	PRO	nd	nd	64.65	84	ALA	7.91	118.54	52.28
35	SER	7.74	111.05	59.22	85	SER	7.26	113.42	59.02
36	LEU	7.55	122.94	57.11	86	ASP	8.45	120.80	54.34
37	LEU	7.52	111.97	52.90	87	LEU	7.88	118.43	55.49
38	ASP	7.55	119.56	56.68	88	GLY	8.06	107.83	46.21
39	GLY	8.71	107.72	44.45	89	LEU	7.99	118.41	52.97
40	ILE	7.32	120.70	60.30	90	ASN	8.94	119.31	50.07
41	VAL	8.50	127.12	60.05	91	PRO	nd	nd	61.80
42	VAL	8.92	123.90	59.51	92	ASN	8.95	117.38	52.28
43	GLU	8.74	127.76	56.77	93	SER	8.79	118.48	57.51
44	TYR	8.18	128.55	56.06	94	ALA	8.45	127.46	51.55
45	TYR	8.86	126.69	59.23	95	GLY	8.72	112.44	46.02
46	GLY	8.33	102.83	44.99	96	SER	8.86	120.85	58.80
47	THR	7.76	117.16	59.35	97	ASP	7.90	119.91	53.25
48	PRO	nd	nd	63.17	98	ILE	8.61	121.89	60.26
49	THR	9.17	126.44	60.37	99	ARG	8.92	126.53	54.28
50	PRO	nd	nd	63.06	100	VAL	9.02	121.18	58.41

Table 1-2. Continued.

	aa	HN	N	Cα		aa	HN	N	Cα
101	PRO	nd	nd	61.26	151	ASP	8.33	119.40	57.12
102	LEU	8.80	124.62	51.24	152	ASP	7.93	120.41	56.90
103	PRO	nd	nd	nd	153	ASP	7.84	120.42	57.06
104	PRO	nd	nd	61.89	154	ARG	8.08	119.74	59.54
105	LEU	8.81	122.92	54.55	155	ARG	8.22	118.84	58.96
106	THR	7.66	112.94	60.07	156	SER	8.10	113.97	60.93
107	GLU	9.00	121.63	59.23	157	GLN	8.40	119.37	59.34
108	GLU	8.70	117.84	59.29	158	ASP	7.77	120.68	57.07
109	ARG	7.70	119.72	57.84	159	ASP	8.36	121.71	57.36
110	ARG	8.60	119.45	60.34	160	VAL	9.14	120.09	66.06
111	LYS	8.19	120.70	59.67	161	GLN	8.66	125.92	58.69
112	ASP	8.14	121.58	57.22	162	LYS	8.11	120.10	59.70
113	LEU	8.74	118.80	57.35	163	LEU	7.78	119.92	57.56
114	THR	8.14	116.08	67.01	164	THR	8.08	118.65	66.73
115	LYS	7.61	121.24	59.76	165	ASP	8.69	120.84	56.95
116	ILE	7.93	120.83	64.69	166	ALA	7.89	121.48	54.58
117	VAL	8.44	117.94	65.70	167	ALA	8.06	122.47	55.05
118	ARG	8.34	120.42	60.17	168	ILE	8.70	117.84	63.94
119	GLY	8.33	109.57	46.73	169	LYS	8.18	119.88	59.75
120	GLU	8.41	122.55	58.36	170	LYS	7.67	119.08	59.79
121	ALA	8.59	124.44	54.41	171	ILE	8.06	122.47	65.54
122	GLU	7.77	118.61	58.50	172	GLU	8.77	117.68	58.47
123	GLN	7.80	116.89	58.43	173	ALA	8.34	122.75	54.55
124	ALA	7.71	123.09	54.48	174	ALA	7.77	120.68	54.18
125	ARG	8.37	117.95	60.20	175	LEU	8.93	120.51	58.00
126	VAL	8.33	118.98	65.98	176	ALA	8.36	120.96	54.74
127	ALA	7.96	122.32	55.21	177	ASP	7.99	118.41	56.72
128	VAL	8.35	119.55	67.05	178	LYS	7.89	121.47	56.18
129	ARG	8.45	119.59	59.94	179	GLU	9.11	118.29	60.30
130	ASN	8.66	121.49	55.32	180	ALA	7.93	120.40	54.72
131	VAL	7.80	122.76	66.26	181	GLU	7.72	119.18	58.89
132	ARG	7.66	120.13	58.97	182	LEU	8.09	117.97	56.63
133	ARG	7.78	117.87	58.71	183	MET	7.59	114.52	55.42
134	ASP	7.98	118.79	57.03	184	GLN	7.61	118.00	56.06
135	ALA	8.54	121.45	54.82	185	PHE	7.67	124.98	58.94
136	ASN	8.47	115.72	54.99					
137	ASP	8.63	122.04	57.16					
138	LYS	8.17	122.57	59.43					
139	VAL	8.11	121.39	66.94					
140	LYS	8.26	119.65	57.89					
141	ALA	7.70	121.72	54.79					
142	LEU	7.40	117.94	57.08					
143	LEU	7.90	121.04	57.53					
144	LYS	8.43	122.91	58.90					
145	ASP	7.50	115.84	53.47					
146	LYS	8.18	114.14	57.05					
147	GLU	8.47	115.72	57.20					
148	ILE	7.16	108.86	58.30					
149	SER	9.10	116.02	56.08					
150	GLU	9.09	120.40	59.58					

Table 1-3. Chemical shift table of *P. aeruginosa* RRF.

	aa	HN	N	Cα		aa	HN	N	Cα
1	MET	nd	nd	nd	51	LEU	8.22	124.25	58.06
2	ILE	nd	nd	66.33	52	ARG	8.83	113.63	57.36
3	ASN	9.10	117.64	56.16	53	GLN	7.92	115.00	56.23
4	GLU	8.37	120.08	60.28	54	VAL	7.75	111.43	60.11
5	ILE	7.59	121.75	64.64	55	ALA	7.70	123.83	49.98
6	LYS	8.02	119.00	60.54	56	ASN	7.96	117.01	51.68
7	LYS	8.21	120.00	59.06	57	VAL	8.68	127.17	61.37
8	GLU	8.21	119.61	58.59	58	THR	9.24	119.06	59.24
9	ALA	7.97	120.65	nd	59	VAL	8.59	121.08	62.10
10	GLN	nd	nd	61.42	60	GLU	8.46	130.05	57.36
11	GLU	8.18	117.17	59.26	61	ASP	8.32	115.16	52.85
12	ARG	8.61	119.05	59.61	62	SER	8.43	109.30	61.23
13	MET	8.61	121.59	60.54	63	ARG	8.34	117.79	55.07
14	GLY	8.22	107.26	47.06	64	THR	7.64	117.77	62.84
15	LYS	8.04	122.55	58.59	65	LEU	8.25	125.82	52.71
16	THR	7.80	119.59	66.80	66	ALA	9.12	123.19	50.43
17	LEU	7.96	125.17	56.11	67	LEU	9.35	121.81	53.59
18	GLU	8.34	122.07	58.75	68	ALA	8.40	126.86	49.92
19	ALA	8.14	122.52	54.68	69	VAL	8.48	123.81	61.77
20	LEU	7.91	122.02	56.99	70	PHE	7.44	124.79	58.74
21	GLY	7.97	105.23	46.79	71	ASP	8.61	119.05	51.69
22	HIS	7.95	119.77	57.72	72	LYS	8.92	125.12	58.72
23	ALA	8.16	123.51	54.83	73	SER	8.71	115.71	60.39
24	PHE	9.16	119.01	56.60	74	MET	8.16	118.87	54.17
25	ALA	7.91	122.02	53.74	75	ILE	7.26	120.08	66.14
26	LYS	7.03	113.28	56.25	76	GLN	8.37	117.82	59.11
27	ILE	7.45	120.41	60.84	77	ALA	8.30	122.92	54.53
28	ARG	7.77	130.03	56.20	78	VAL	8.29	120.30	66.40
29	THR	7.91	108.21	59.77	79	GLU	8.40	118.99	60.41
30	GLY	8.67	107.81	44.98	80	LYS	8.43	118.15	58.88
31	ARG	7.88	118.92	53.63	81	ALA	7.94	122.50	54.39
32	ALA	8.35	124.68	52.15	82	ILE	7.87	115.82	64.47
33	HIS	7.36	118.46	52.75	83	MET	8.39	119.64	58.67
34	PRO	nd	nd	65.21	84	THR	8.07	107.83	62.16
35	SER	8.38	111.12	59.43	85	SER	7.26	116.86	59.38
36	ILE	7.70	122.91	62.60	86	ASP	8.52	120.22	54.48
37	LEU	7.50	115.37	53.21	87	LEU	7.84	117.67	55.14
38	ASP	7.74	120.25	57.30	88	GLY	8.14	107.84	46.12
39	SER	8.17	111.36	58.08	89	LEU	7.67	117.76	52.81
40	VAL	7.42	123.08	63.22	90	ASN	8.98	119.38	49.90
41	MET	8.54	127.11	52.28	91	PRO	nd	nd	61.74
42	VAL	9.21	120.51	59.67	92	ALA	8.94	123.49	50.84
43	SER	8.46	121.58	57.39	93	THR	8.73	119.79	62.13
44	TYR	8.74	129.83	56.87	94	ALA	8.81	131.04	51.10
45	TYR	8.73	125.94	58.94	95	GLY	8.89	115.13	46.62
46	GLY	8.24	103.66	45.01	96	THR	8.58	116.50	60.84
47	ALA	7.66	122.95	50.24	97	THR	7.96	117.47	61.37
48	ASP	8.75	125.20	54.29	98	ILE	8.61	124.92	59.79
49	THR	9.19	122.52	59.53	99	ARG	9.14	127.33	54.77
50	PRO	nd	nd	63.31	100	VAL	9.08	120.91	58.30

Table 1-3. Continued.

	aa	HN	N	Cα		aa	HN	N	Cα
101	PRO	nd	nd	61.30	151	ASP	8.48	118.92	57.24
102	MET	8.75	121.03	51.05	152	GLU	7.92	119.28	58.83
103	PRO	nd	nd	62.22	153	GLU	8.52	120.80	59.83
104	ALA	8.41	124.33	51.57	154	ARG	8.34	120.65	59.03
105	LEU	8.63	122.43	54.01	155	ARG	8.07	119.30	59.01
106	THR	8.12	113.11	59.92	156	ALA	8.13	120.84	54.28
107	GLU	9.04	121.88	59.41	157	GLY	8.67	107.81	46.75
108	GLU	8.63	117.46	59.24	158	ASP	8.12	124.22	56.97
109	THR	7.79	117.04	65.01	159	ASP	7.97	121.19	57.32
110	ARG	8.63	122.43	60.43	160	VAL	8.50	121.24	66.13
111	LYS	8.32	120.41	59.55	161	GLN	8.81	125.77	58.94
112	GLY	8.00	108.33	46.94	162	LYS	8.25	119.89	59.38
113	TYR	8.62	122.72	57.85	163	LEU	7.89	121.25	57.75
114	THR	nd	nd	nd	164	THR	nd	nd	nd
115	LYS	7.83	121.75	58.73	165	ASP	8.56	120.45	57.16
116	GLN	8.08	120.54	58.59	166	LYS	8.02	122.26	59.01
117	ALA	8.55	121.92	54.74	167	PHE	nd	nd	nd
118	ARG	8.25	116.37	59.78	168	ILE	9.24	121.37	63.63
119	ALA	8.30	123.99	54.84	169	GLY	8.17	108.03	46.84
120	GLU	8.50	119.55	58.25	170	GLU	8.02	121.45	58.81
121	ALA	8.63	122.43	54.99	171	ILE	8.29	123.36	65.63
122	GLU	8.12	118.52	58.70	172	GLU	8.02	118.36	58.30
123	GLN	7.89	118.05	58.35	173	LYS	8.16	118.87	58.87
124	ALA	7.81	122.37	54.65	174	ALA	8.09	122.63	54.49
125	ARG	8.44	119.26	60.21	175	LEU	8.91	121.35	57.87
126	VAL	8.39	119.64	66.17	176	GLU	8.69	118.86	59.01
127	SER	nd	nd	nd	177	ALA	7.86	121.19	54.40
128	VAL	8.44	119.78	67.37	178	LYS	7.82	120.44	56.47
129	ARG	8.53	119.13	60.12	179	GLU	8.94	117.34	59.85
130	ASN	8.63	122.43	55.27	180	ALA	7.97	120.65	54.64
131	ILE	8.30	123.99	65.16	181	ASP	7.67	119.00	56.60
132	ARG	8.07	120.84	59.46	182	LEU	7.89	118.53	56.53
133	ARG	7.96	118.84	59.30	183	MET	7.55	116.00	55.11
134	ASP	8.29	120.61	56.74	184	ALA	7.55	123.45	52.55
135	ALA	8.24	122.94	54.52	185	VAL	7.77	123.54	63.32
136	LEU	8.60	116.22	57.61					
137	ALA	8.20	123.04	54.77					
138	GLN	7.99	118.73	58.69					
139	LEU	8.21	120.34	57.54					
140	LYS	8.11	120.18	58.43					
141	ASP	8.00	120.05	57.11					
142	LEU	7.58	117.57	57.23					
143	GLN	7.86	121.60	58.67					
144	LYS	8.73	123.17	59.06					
145	GLU	7.72	115.54	55.44					
146	LYS	8.09	113.68	56.92					
147	GLU	8.32	116.45	57.09					
148	ILE	7.01	107.83	58.05					
149	SER	9.17	118.14	56.35					
150	GLU	9.22	120.89	59.76					

Table 1-4. Chemical shift table of *T. maritima* RRF.

	aa	HN	N	Cα		aa	HN	N	Cα
1	MET	nd	nd	nd	51	VAL	8.37	121.86	66.59
2	VAL	nd	nd	nd	52	ASN	8.45	113.97	54.67
3	ASN	nd	nd	nd	53	GLN	7.67	116.22	56.12
4	PRO	nd	nd	nd	54	LEU	7.50	117.03	53.89
5	PHE	8.42	117.33	61.30	55	ALA	7.25	120.21	51.00
6	ILE	7.54	118.95	63.22	56	THR	7.67	113.18	61.55
7	LYS	7.89	120.17	60.08	57	ILE	8.82	127.49	60.11
8	GLU	7.96	118.50	59.27	58	SER	8.91	121.43	56.64
9	ALA	8.03	120.17	55.64	59	ILE	8.53	122.35	60.57
10	LYS	8.64	116.65	60.88	60	SER	8.77	122.56	57.12
11	GLU	8.19	117.96	59.59	61	GLU	8.65	121.35	56.95
12	LYS	8.21	118.37	60.27	62	GLU	8.54	115.80	59.50
13	MET	8.69	121.55	61.02	63	ARG	8.57	116.58	56.47
14	LYS	8.31	120.65	61.02	64	THR	7.63	113.84	61.83
15	ARG	7.87	117.88	59.07	65	LEU	9.08	125.86	53.53
16	THR	7.56	117.41	67.64	66	VAL	9.17	124.05	61.80
17	LEU	8.14	122.84	58.90	67	ILE	9.31	127.51	60.58
18	GLU	8.46	117.55	59.46	68	LYS	8.74	127.85	52.59
19	LYS	7.84	120.78	59.35	69	PRO	nd	nd	61.91
20	ILE	8.02	121.26	63.17	70	TRP	7.35	121.18	58.45
21	GLU	8.84	119.11	61.10	71	ASP	8.34	120.19	52.10
22	ASP	8.13	120.31	57.79	72	LYS	8.87	123.78	59.28
23	GLU	8.21	119.17	59.56	73	SER	8.79	116.22	61.50
24	LEU	8.45	117.81	57.72	74	VAL	7.64	115.59	61.85
25	ARG	8.04	120.33	58.88	75	LEU	7.60	123.59	59.61
26	LYS	7.26	115.56	57.11	76	SER	8.48	111.64	61.49
27	MET	7.03	118.81	56.32	77	LEU	7.09	120.64	57.46
28	ARG	8.27	127.68	56.64	78	ILE	8.11	120.49	65.84
29	THR	8.38	116.26	59.74	79	GLU	8.17	120.65	60.87
30	GLY	8.21	108.79	46.01	80	LYS	7.86	117.04	59.75
31	LYS	7.65	121.03	53.26	81	ALA	7.79	121.59	54.89
32	PRO	nd	nd	nd	82	ILE	8.32	117.59	65.13
33	SER	nd	nd	nd	83	ASN	8.42	121.31	56.04
34	PRO	nd	nd	64.66	84	ALA	7.69	119.99	52.57
35	ALA	7.83	119.77	54.56	85	SER	7.49	115.45	59.02
36	ILE	7.22	112.08	63.15	86	ASP	8.35	118.52	53.48
37	LEU	7.39	116.63	54.23	87	LEU	8.13	118.57	57.25
38	GLU	7.42	119.02	59.74	88	GLY	8.60	106.52	46.40
39	GLU	7.98	113.42	55.78	89	LEU	6.92	117.26	52.76
40	ILE	7.37	121.20	60.52	90	ASN	8.49	119.89	50.45
41	LYS	8.35	126.10	54.39	91	PRO	nd	nd	62.51
42	VAL	8.66	118.08	59.33	92	ILE	8.61	123.98	60.78
43	ASP	8.51	125.55	54.39	93	ASN	9.00	128.28	51.57
44	TYR	7.98	128.26	56.33	94	ASP	8.42	126.02	52.90
45	TYR	8.40	124.34	59.49	95	GLY	8.97	110.05	45.43
46	GLY	7.90	97.94	45.30	96	ASN	8.96	118.95	55.31
47	VAL	7.46	121.27	59.31	97	VAL	9.12	112.49	58.96
48	PRO	nd	nd	nd	98	ILE	8.17	116.32	58.23
49	THR	nd	nd	nd	99	ARG	8.96	125.61	54.63
50	PRO	nd	nd	62.71	100	LEU	9.10	122.99	53.17

Table 1-4. Continued.

	aa	HN	N	Cα		aa	HN	N	Cα
101	VAL	8.90	125.93	62.18	151	ASP	8.93	116.65	57.48
102	PHE	9.11	129.64	55.80	152	ASP	7.22	120.11	57.11
103	PRO	nd	nd	nd	153	ALA	8.34	122.94	55.91
104	SER	nd	nd	nd	154	LYS	7.99	117.76	59.10
105	PRO	nd	nd	nd	155	ARG	7.53	120.13	59.86
106	THR	nd	nd	nd	156	LEU	8.45	120.19	58.10
107	THR	nd	nd	67.03	157	GLU	8.35	119.19	60.26
108	GLU	8.47	120.33	59.78	158	ASN	7.87	117.88	56.48
109	GLN	7.48	119.57	58.52	159	GLU	8.32	120.98	59.78
110	ARG	7.83	116.70	60.58	160	ILE	8.67	119.64	62.75
111	GLU	8.01	116.60	59.78	161	GLN	8.57	125.46	59.64
112	LYS	7.65	120.24	59.77	162	LYS	7.94	119.49	59.48
113	TRP	8.38	122.12	58.83	163	LEU	7.96	119.96	58.09
114	VAL	8.79	120.97	68.22	164	THR	8.10	115.76	67.92
115	LYS	7.91	119.33	59.74	165	ASP	8.23	120.78	57.93
116	LYS	8.04	120.39	58.51	166	GLU	8.18	120.92	59.60
117	ALA	8.58	121.19	55.34	167	PHE	8.50	118.78	63.95
118	LYS	8.64	118.40	58.89	168	ILE	8.70	121.31	65.02
119	GLU	8.13	119.78	59.81	169	GLU	7.99	118.98	59.73
120	ILE	8.24	120.79	65.46	170	LYS	8.02	119.77	58.71
121	VAL	8.11	119.15	67.74	171	LEU	8.11	121.14	58.45
122	GLU	9.08	121.41	59.82	172	ASP	8.04	119.59	58.25
123	GLU	8.12	120.53	59.78	173	GLU	8.10	121.53	59.87
124	GLY	8.03	109.18	47.84	174	VAL	8.35	117.62	66.14
125	LYS	8.45	122.16	60.91	175	PHE	8.24	120.40	61.81
126	ILE	7.85	119.63	65.40	176	GLU	8.17	119.42	59.58
127	ALA	7.74	122.53	55.63	177	ILE	8.08	119.47	64.90
128	ILE	8.35	118.89	63.22	178	LYS	7.76	122.34	56.90
129	ARG	8.32	118.94	60.62	179	LYS	8.92	120.36	60.32
130	ASN	8.69	121.43	56.05	180	GLU	7.78	118.10	59.69
131	ILE	8.12	123.91	65.52	181	GLU	7.62	119.74	59.49
132	ARG	7.78	118.81	60.31	182	ILE	8.46	119.15	65.26
133	ARG	7.88	117.10	59.96	183	MET	8.15	114.26	55.56
134	GLU	8.19	119.12	59.43	184	GLU	7.83	118.27	57.49
135	ILE	8.33	120.48	63.68	185	PHE	7.51	124.61	60.50
136	LEU	8.55	119.68	58.30					
137	LYS	7.73	118.92	59.83					
138	LYS	7.29	119.40	59.53					
139	ILE	7.97	119.78	65.70					
140	LYS	7.99	117.88	58.93					
141	GLU	8.15	121.15	59.54					
142	ASP	8.23	122.03	57.56					
143	GLN	8.79	122.75	59.53					
144	LYS	8.31	122.99	59.47					
145	GLU	7.67	116.25	56.30					
146	GLY	7.89	106.54	45.48					
147	LEU	8.17	118.82	56.15					
148	ILE	6.78	115.12	57.81					
149	PRO	nd	nd	62.59					
150	GLU	8.89	123.18	60.56					

Table 1-5. Chemical shift table of *T. thermophilus* RRF.

	aa	HN	N	Cα		aa	HN	N	Cα
1	MET	nd	nd	nd	51	PRO	nd	nd	nd
2	THR	nd	nd	nd	52	LEU	8.71	125.44	59.93
3	LEU	8.66	120.54	58.06	53	ASN	8.11	111.53	54.78
4	LYS	7.95	115.53	60.16	54	GLN	8.08	117.61	57.32
5	GLU	7.60	119.38	59.12	55	ILE	7.62	109.79	60.33
6	LEU	7.99	123.93	58.31	56	ALA	7.80	124.18	51.33
7	TYR	8.66	123.30	58.67	57	THR	8.61	110.63	60.38
8	ALA	8.00	121.58	55.47	58	VAL	8.61	123.52	60.55
9	GLU	8.68	120.75	59.45	59	THR	8.90	118.28	59.75
10	THR	8.14	116.85	68.10	60	ALA	8.64	123.25	58.67
11	ARG	8.17	119.64	60.41	61	PRO	nd	nd	nd
12	SER	8.15	114.03	61.86	62	ASP	7.77	115.01	52.58
13	HIS	8.48	120.34	58.67	63	PRO	nd	nd	nd
14	MET	8.22	120.95	60.90	64	ARG	8.43	115.77	54.83
15	GLN	8.53	121.03	58.94	65	THR	7.38	118.27	62.66
16	LYS	7.74	119.19	59.15	66	LEU	8.72	121.72	52.74
17	SER	7.62	115.53	62.97	67	VAL	8.92	121.42	60.70
18	LEU	8.35	124.90	57.52	68	VAL	8.96	127.44	60.37
19	GLU	8.25	120.11	59.56	69	GLN	8.58	125.01	54.77
20	VAL	7.83	121.77	66.75	70	SER	8.26	114.59	57.36
21	LEU	7.53	121.02	58.56	71	TRP	7.56	123.68	58.05
22	GLU	8.84	119.18	60.66	72	ASP	7.80	120.04	52.32
23	HIS	8.31	119.41	59.48	73	GLN	nd	nd	nd
24	ASN	8.46	120.04	55.37	74	ASN	8.54	117.00	55.85
25	LEU	8.43	117.81	57.35	75	ALA	7.83	123.02	54.25
26	ALA	8.16	120.93	54.40	76	LEU	7.40	116.56	58.57
27	GLY	7.22	128.48	45.32	77	LYS	7.79	118.02	59.39
28	LEU	7.07	119.47	54.05	78	ALA	7.56	123.57	55.01
29	ARG	8.59	125.39	nd	79	ILE	8.49	121.30	65.55
30	THR	8.03	111.11	nd	80	GLU	8.52	120.91	60.91
31	GLY	8.51	108.14	45.92	81	LYS	7.55	118.36	59.67
32	ARG	7.66	118.15	54.42	82	ALA	7.84	120.05	55.02
33	ALA	8.67	125.43	53.41	83	ILE	8.42	116.12	65.62
34	ASN	7.82	121.01	49.83	84	ARG	8.61	123.32	60.48
35	PRO	nd	nd	nd	85	ASP	8.44	117.31	55.21
36	ALA	7.99	117.06	54.72	86	SER	7.46	115.99	59.38
37	LEU	7.73	116.70	57.24	87	ASP	8.40	118.56	53.96
38	LEU	7.23	110.99	54.16	88	LEU	8.08	118.13	56.70
39	LEU	7.20	115.63	58.64	89	GLY	8.42	107.99	46.60
40	HIS	8.11	113.20	55.27	90	LEU	7.49	117.16	53.07
41	LEU	7.26	123.41	55.73	91	ASN	nd	nd	nd
42	LYS	8.34	123.34	55.73	92	PRO	nd	nd	nd
43	VAL	9.18	123.90	60.66	93	SER	8.87	116.12	56.93
44	GLU	8.46	127.81	56.51	94	ASN	nd	nd	nd
45	TYR	9.06	130.29	57.16	95	LYS	8.51	126.59	55.36
46	TYR	8.65	125.17	59.20	96	GLY	8.98	113.28	46.96
47	GLY	8.44	130.78	45.65	97	ASP	8.43	119.67	53.58
48	ALA	7.62	123.54	50.37	98	ALA	7.48	119.01	51.32
49	HIS	8.49	120.09	56.36	99	LEU	8.78	117.00	52.88
50	VAL	9.16	121.28	57.77	100	TYR	9.11	123.25	57.74

Table 1-5. Continued.

	aa	HN	N	Cα		aa	HN	N	Cα
101	ILE	9.39	124.65	60.46	151	GLU	nd	nd	nd
102	ASN	8.79	126.05	53.12	152	ASP	nd	nd	nd
103	ILE	8.71	127.34	56.23	153	GLU	7.94	119.51	59.42
104	PRO	nd	nd	nd	154	THR	8.50	118.19	67.86
105	PRO	nd	nd	nd	155	LYS	8.35	122.24	59.61
106	LEU	8.65	121.18	54.68	156	ARG	8.01	120.40	59.57
107	THR	7.63	111.89	60.46	157	ALA	7.88	124.50	54.74
108	GLU	nd	nd	nd	158	GLU	8.55	119.68	60.23
109	GLU	8.79	117.75	59.95	159	ALA	7.97	121.47	54.85
110	ARG	7.57	119.46	58.20	160	GLU	8.13	122.33	59.11
111	ARG	8.48	119.10	60.81	161	ILE	8.21	119.21	64.80
112	LYS	7.88	116.93	60.03	162	GLN	8.52	123.87	59.05
113	ASP	7.80	120.48	57.53	163	LYS	8.25	121.27	60.00
114	LEU	8.46	122.10	57.90	164	ILE	8.23	120.98	66.15
115	VAL	8.33	119.76	67.89	165	THR	7.98	115.84	68.17
116	ARG	7.71	119.18	59.98	166	ASP	8.88	121.08	57.70
117	ALA	7.81	122.32	55.24	167	GLU	8.08	122.19	59.26
118	VAL	8.41	118.84	67.31	168	PHE	8.19	118.76	64.31
119	ARG	8.21	117.20	59.82	169	ILE	9.15	122.22	63.79
120	GLN	8.33	122.10	58.98	170	ALA	7.84	119.75	55.30
121	TYR	8.60	119.19	59.92	171	LYS	7.72	118.18	59.90
122	ALA	9.17	122.93	55.92	172	ALA	8.45	124.86	55.76
123	GLU	8.03	119.08	59.16	173	ASP	8.77	118.30	57.59
124	GLU	8.24	118.89	59.92	174	GLN	8.14	119.91	59.09
125	GLY	8.39	108.44	47.21	175	LEU	8.08	120.79	58.10
126	ARG	8.61	121.82	60.98	176	ALA	8.13	121.40	55.41
127	VAL	8.81	120.25	66.91	177	GLU	8.46	119.70	59.72
128	ALA	7.96	122.46	55.65	178	LYS	8.13	118.45	59.29
129	ILE	8.29	119.99	66.26	179	LYS	7.78	119.87	56.77
130	ARG	8.80	119.73	60.73	180	GLU	8.58	119.63	61.47
131	ASN	8.75	122.26	56.24	181	GLN	8.14	116.48	58.88
132	ILE	8.03	123.46	65.09	182	GLU	7.81	119.92	59.04
133	ARG	8.10	121.42	60.23	183	ILE	7.92	119.74	64.98
134	ARG	7.77	118.64	60.00	184	LEU	8.02	117.88	56.18
135	GLU	8.09	119.36	59.61	185	GLY	7.60	113.21	46.66
136	ALA	8.86	124.22	55.48					
137	LEU	8.55	118.26	57.63					
138	ASP	8.09	122.48	57.76					
139	LYS	8.23	121.75	60.19					
140	LEU	8.80	121.50	57.88					
141	LYS	7.74	117.90	59.93					
142	LYS	7.13	118.14	59.30					
143	LEU	8.53	122.16	57.84					
144	ALA	9.26	120.19	55.37					
145	LYS	7.02	115.60	58.37					
146	GLU	7.80	120.40	59.14					
147	LEU	8.50	114.98	54.41					
148	HIS	7.44	115.93	56.48					
149	LEU	8.03	116.87	54.99					
150	SER	9.28	119.09	57.32					

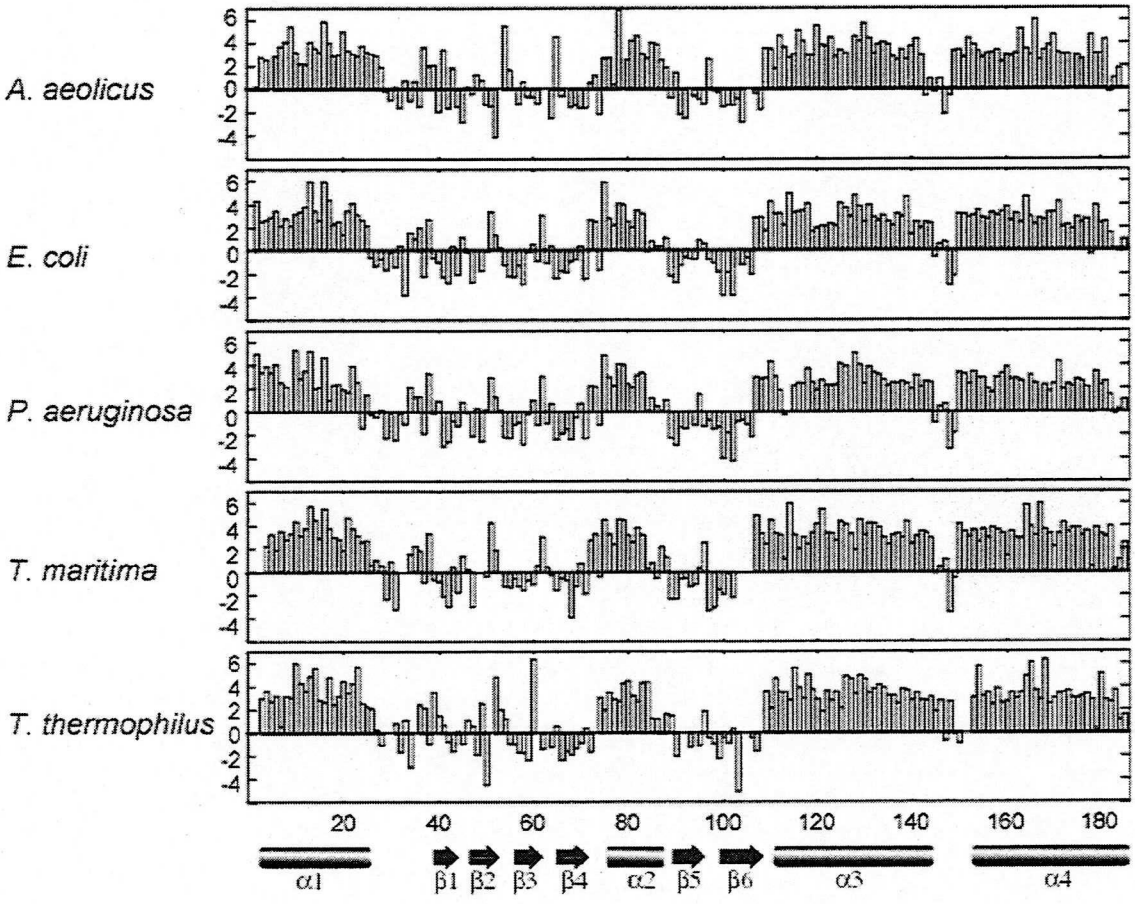

Figure 1-1. The differences between observed and standard chemical shifts of α carbons for RRFs from five baceria. Summary of the consensus secondary structure elements are indicated in bottom.

Chapter II

Solution Structure of the Ribosome Recycling Factor from *Aquifex aeolicus*

The recent impressive progress in structural biology of translation machinery has yielded insights into the mechanism of protein biosynthesis. Structures of ribosome and its subunits have been elucidated by cryo-electron microscopy and x-ray analysis on their crystals. As shown in Figure 2-1, the x-ray crystallography (*29-31*) revealed the overall arrangement of the proteins and RNAs in the ribosome providing the location of the three essential sites, aminoacyl-tRNA binding (A-site), peptidyl-tRNA binding (P-site), and exit (E-site) sites. Furthermore, recent crystallographic studies revealed the crystal structure of both ribosomal subunits at very high resolutions (*32-34*). Furthermore, soluble proteins involved in the translation process were elucidated at atomic resolution by x-ray crystallography and NMR spectroscopy (*35-38*).

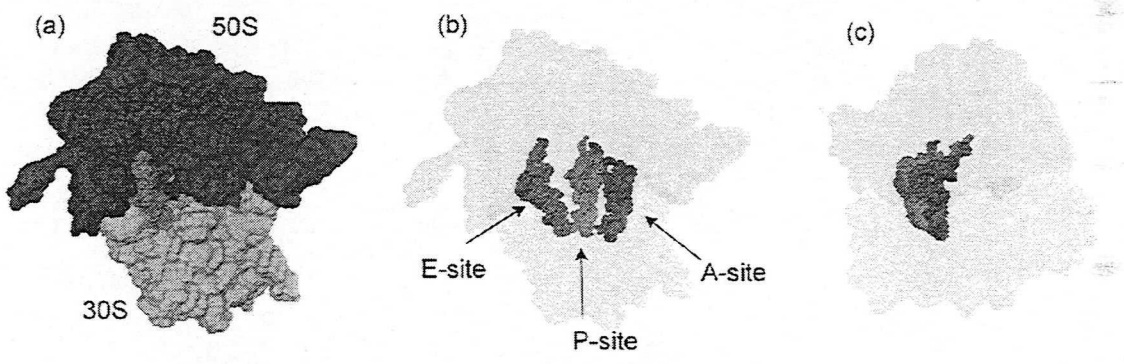

Figure 2-1. Three dimensional structure of the ribosome. (a) Surface model of the ribosome, A-site tRNA, P-site tRNA, and E-site tRNA. (b) Same view of (a) with transparent representation of the ribosome. (c) A-site side view of (b).

Recently, three-dimensional structures of RRF from several bacteria; *Thermotoga maritima* (*15*), *Escherichia coli* (*16*), *Thermus thermophilus* (*17*), and *Vivrio parahaemolyticus* (*19*) have been determined by X-ray crystallography also. All of these structures consist of two domains; domain I displays a three-helix bundle structure and domain II exists as a three layer β/α/β sandwich structure. As shown in Figure 2-2, except for a crystal structure of detergent-bound RRF from *E. coli*, the two domains are arranged in a L-shape, such that the overall structures are very similar to that of tRNA in terms of shape and dimensions. Based

on this similarity, a concept of molecular mimicry was proposed (*15*). However, the azimuth angles between domains are different each other (*19*). In other words, when the long axis of domain I is set as the z-axis, the long axis of domain II distributed in the xy-plane. Such differences in the arrangement of domains suggests that the joint region between domains is flexible and the observed arrangements in crystal were interfered by packing force. Thus, the structural analysis of RRF molecule in solution is quite important to establish the structure-function relationship of RRF. In this chapter, the author reports the three dimensional structure of RRF from *Aquifex aeolicus* in solution as determined by NMR. The author successfully showed that the L-shaped conformation with the domains, which has been observed in crystal state, is maintained even in solution.

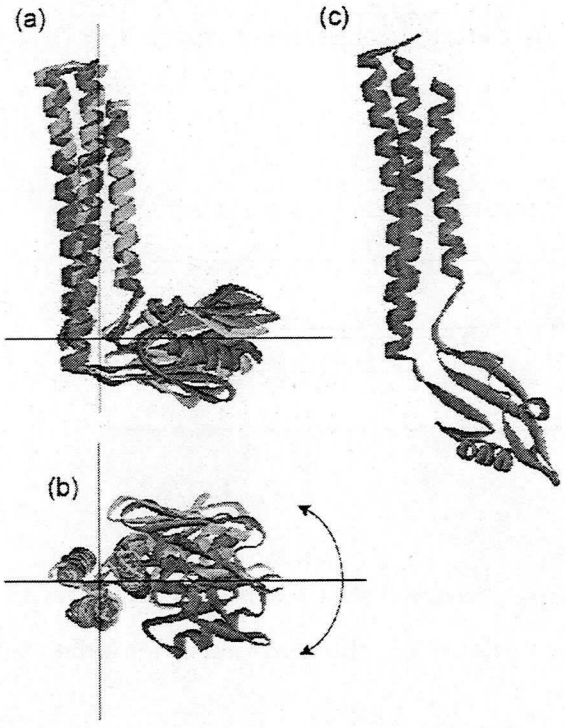

Figure 2-2. X-ray structures of RRFs. (a) RRFs from *T. maritima* (red), *T. thermophilus* (green), and *V. parahaemolyticus* (blue) are superimposed over domain I. (b) Top view of (a). (c) RRF from *E. coli*.

Experimental Procedures

NMR spectroscopy

NMR experiments were carried out at 40 °C on Varian INOVA600 or INOVA500 spectrometers. ^{15}N-separated NOESY-HSQC and ^{15}N-seperated TOCSY spectra were acquired on [U-^{15}N]RRF. HBHA(CBCACO)NH, H(CCO)NH, HCCH-TOCSY, HCCH-COSY, ^{13}C-^{1}H HSQC, (Hβ)Cβ(CγCδ)Hδ, ^{13}C-separated NOESY-HSQC, J-modulated HSQC spectra were acquired on [U-^{15}N/^{13}C]RRF. HN(CA)CO, C(CO)NH and ^{15}N-separated HMQC-NOESY-HSQC spectra were acquired on [U-^{2}H/^{15}N/^{13}C]RRF. The mixing times employed for NOE experiments were 75ms except for 3D ^{15}N-separated HMQC-NOESY-HSQC, for which 150ms was used. A constant time HSQC was acquired on [U-10% ^{13}C]RRF. Slowly water-exchanging ^{1}HN were identified from a series of ^{15}N-HSQC spectra following a rapid buffer exchange to 99% D_2O using a NAP-5 column (Amersham Pharmacia Biotech, Uppsala).

The backbone ^{15}N relaxation parameters comprising the ^{15}N longitudinal relaxation time T_1, transverse relaxation time T_2 and ^{15}N-{^{1}H} *NOE*, were measured using HSQC type pulse sequences. The T_1 relaxation decay was sampled at six time points (30, 234, 438, 642, 846 and 1050 ms) and the $T_1\rho$ decay was sampled at five points (12, 24, 36, 48, and 60 ms) using a ^{15}N spin-lock field strength of 2.2 kHz. The ^{15}N-{^{1}H} *NOE* values were derived from two series of spectra, recorded with and without 3.5 s of saturation of the amide protons, respectively. All data were recorded in an interleaved manner in order to minimize the effects of spectrometer drift. The ^{15}N-{^{1}H} *NOE* values were corrected for the finite delay between scans using T_1 values of ^{1}HN, which were estimated by a preliminary experiment (*39*). The T_1 and $T_1\rho$ values were obtained by nonlinear least-squares fitting of a two-parameter monoexponential function through the peak intensities, using the Levenberg-Marquardt algorithm (*40*). The T_2 values were calculated from T_1 and $T_1\rho$ with the resonance offset frequencies and the strength of the spin-lock field (*41*). Uncertainties in T_1 and $T_1\rho$ values were estimated from the covariance matrix of a least-square fit. And those in *NOE* values were estimated by simple error propagation calculation based on baseplane rms noise in spectra.

Structure Calculations

NOEs were classified as strong, medium, weak, or very weak, corresponding to distance restraints of 1.8-2.7 Å (1.8-2.9 Å for NOEs involving amide protons), 1.8-3.3 Å (1.8-3.5 Å for NOEs involving amide protons), 1.8-5.0 Å and 1.8-6.0 Å, respectively (*42*). For distances involving methyl groups, methylene protons and aromatic ring protons, $<r^{-6}>^{-1/6}$ averaged distances were used (*43*). Protein backbone hydrogen-bonding restraints (two per hydrogen bond: one between the amide proton and the carbonyl oxygen of 1.5-2.8 Å and one between the amide nitrogen and the carbonyl oxygen of 2.4-3.5 Å) were introduced (*44*). To collect all the distance restraints, an iterative refinement strategy (*45*) was employed. The program TALOS (*46*) was used to derive the backbone φ and ψ torsion angle restraints based on chemical shifts of Cα, Cβ, C', Hα, and N. The TALOS-derived torsion angles are empirical and may contain a few errors. Therefore, the sufficiently larger ranges (±30°) were employed for TALOS-derived restraints in the initial round of calculation. In the final round of calculation, after the structures were well defined and erroneous restraints were excluded, the minimum ranges employed for φ and ψwere reduced to ±1.5×SD, where SD is the standard deviation for predicted values. χ1 angles for aromatic residues and for Ile, Thr and Val residues were derived from $^{3}J_{C\gamma N}$ and $^{3}J_{C\gamma CO}$ coupling constants (*47, 48*). The minimum ranges employed for χ1 were ±20°.

The preliminary structure calculation using restraints of NOE-derived interproton distances and torsion angles indicated that the structure of *A. aeolicus* RRF has a highly anisotropic prolate shape. Since the anisotropy of the molecule was also shown in the observed profile of T_1 and T_2 data, the author employed the dependence of T_1/T_2 on the rotational diffusion anisotropy as restraints for further structure refinement procedure. The diffusion anisotropy restraints were derived as follows: The initial diffusion tensor was estimated from the examination of histogram of ^{15}N T_1/T_2 ratios for isotropically oriented vectors (*49*). After calculating an ensemble of structures, the diffusion tensor and its unique axis were refined by simplex nonlinear optimization to fit the observed T_1/T_2 ratios to the calculated T_1/T_2 ratios derived from structures. In this procedure, a fully asymmetric diffusion tensor was used. The structures were calculated using the program CNS (*50*) with torsion angle dynamics (*51*) followed by a simulated annealing refinement on a Linux workstation. The final structures were analyzed using the programs of MOLMOL (*52*) and PROCHECK (*53*).

Results

Resonance Assignments

Procedures and results of backbone assignments are mentioned in chapter 1. Hα/β resonances were assigned in HBHA(CBCACO)NH and ^{15}N-separated TOCSY-HSQC spectra. Other aliphatic ^{13}C and ^{1}H side chain assignments were obtained mainly from C(CO)NH and H(CCO)NH spectra. Because of the relatively low sensitivities for these experiments, HCCH-TOCSY and HCCH-COSY spectra were employed to complement them. Aromatic side chain assignments were obtained from (Hβ)Cβ(CγCδ)Hδ spectrum. Most ^{1}H and ^{13}C resonances of the side chain were assigned. In some cases, side chain resonances of residues with longer side chains could not be assigned unambiguously because of overlapping signals. Stereo-specific assignments for pro-chiral methyl resonances of Leu and Val were obtained in constant-time HSQC spectrum recorded on [*U*-10% ^{13}C] RRF (*54*). No stereo-specific assignment for methylene protons was obtained.

T_1/T_2 restraint

T_1, T_2 and ^{15}N-{^{1}H} *NOE* values for 139 out of 173 assigned backbone nitrogen nuclei were analyzed to derive T_1/T_2 restraints, whereas peak overlap prevented the analysis of cross peaks for 34 residues. In the absence of significant internal motions, the ^{15}N T_1/T_2 ratio provides the long-range structural information in the form of internal ^{15}N-^{1}H vector constraints with respect to an overall molecular reference frame. Residues with large-amplitude internal motions on subnanosecond time scale were recognized by significant decreases in ^{15}N-{^{1}H} *NOE* values. Thirty one residues which showed low ^{15}N-{^{1}H} *NOE* values (<0.65) were excluded in the analysis of diffusion tensor (*55*). Furthermore residues undergoing conformational exchange, which can be characterized by $[(\langle T_2\rangle - T_2)/\langle T_2\rangle] - [(\langle T_1\rangle - T_1)/\langle T_1\rangle] > 1.5\times SD$, can be excluded, where SD is the standard deviation of the left-hand side of the equation and $\langle T_1\rangle$ and $\langle T_2\rangle$ are the average values of T_1 and T_2, respectively (*55*). However, such residues were not found in *A. aeolicus* RRF. T_1 and T_2 values of 108 NH cross peaks were utilized to derive an anisotropic rotational diffusion tensor and T_1/T_2 restraints (Figure 2-3a). The histogram of T_1/T_2 (Figure 2-3b) had a bimodal profile and the maximum of the T_1/T_2 ratio was about 3.2 times larger than the minimum ratio. Initial estimates of the effective correlation time, anisotropy and rhombicity from the analysis of a histogram of T_1/T_2 ratios using a fully anisotropic diffusion model, were 13.4 ns, 2.75 and 0.25, respectively. The value of anisotropy is found to be sufficiently large to employ the

T_1/T_2 restraints. Thus, this method has been justified for structure elucidation of *A. aeolicus* RRF.

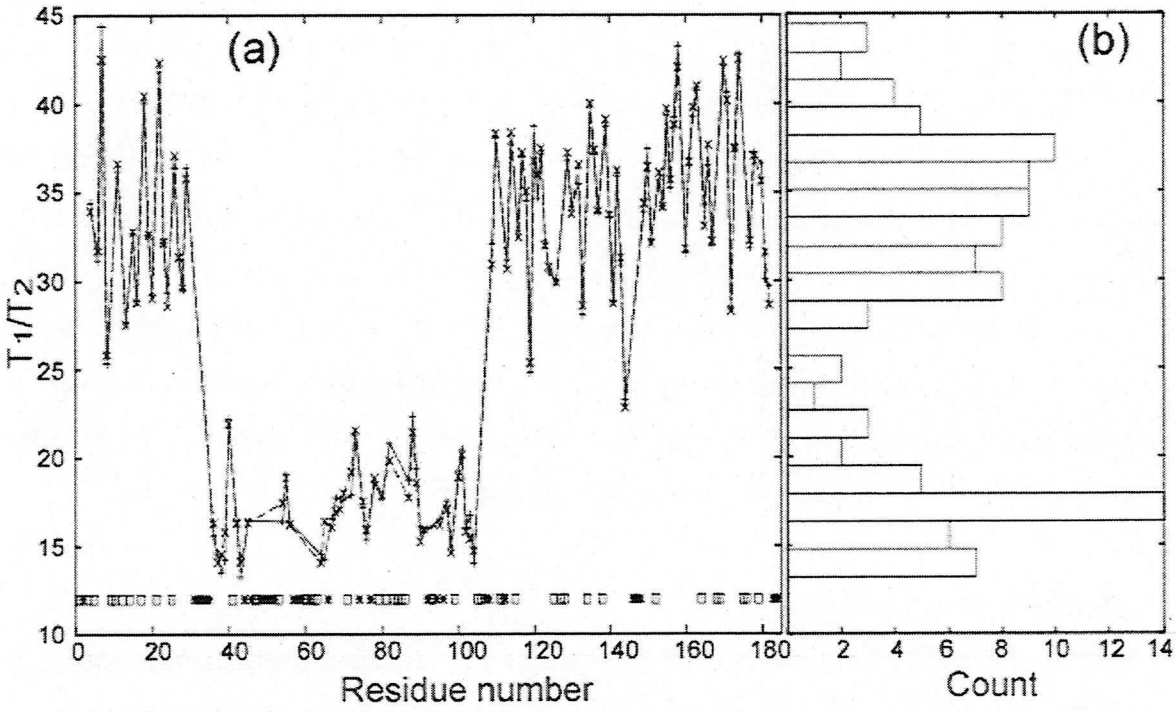

Figure 2-3. (a) Observed (+) and calculated (×) T_1/T_2 ratios versus residue number. Residues with low ^{15}N-{^{1}H} *NOE* values (< 0.65), which were excluded in the analysis of rotational diffusion anisotropy, are indicated by asterisks. Residues with resonance overlap and proline residues are indicated by open-boxes. (b) The histogram of observed T_1/T_2 ratios. The range of T_1/T_2 ratios are divided into twenty bins. The counts of T_1/T_2 ratio in each bin are shown.

Structure Determination.

A total of 1687 distance restraints derived from NOE experiments were employed for structure calculations, including 549 intraresidue, 496 sequential, 386 medium-range and 256 long-range restraints. In addition, 98 H^N-O and N-O hydrogen bond restraints were used in the later stages of the structure calculation. Torsion angle restraints comprised 25 χ_1 restraints derived from semi-quantitative analysis of $^3J_{C\gamma N}$ and $^3J_{C\gamma CO}$ and 301 φ/ψ angle restraints calculated by the program TALOS. Figure 2-4 shows the best-fit superpositions of the backbone traces of 15 structures of *A. aeolicus* RRF obtained by the simulated annealing refinement. The ensemble of 15 structures has no distance restraint violations above 0.5 Å, and no torsion angle restraint violations above 5°. The coordinates of these structures with

experimental restraints were deposited in the Protein Data Bank (PDB: 1GE9). The structure statistics are summarized in Table 2-1. The Ramachandran plot shows that 86.0% of the nonglycine and nonproline residues are found in the most favored region, 11.7% in the additionally allowed regions.

The lowest energy structure among the 15 final structures is shown as a ribbon representation in Figure 2-5a. The resulting structure of *A. aeolicus* RRF has an L-shaped conformation with two domains. The overall structure is very similar to that of tRNA (Figure 2-5b) in shape with nearly the same dimension. Domain I, the leg portion of the molecule corresponding to the vertical line of L, is a three-stranded antiparallel α–helix bundle with length of 60 Å consisting of residues 4-28 (helix 1), 109-142 (helix 3) and 149-181 (helix 4). Each helix is nearly straight and packed together in a slightly right-handed twist with helix-crossing angle of 5°. The H-N vectors of peptide plane in the three-helix bundle are nearly parallel to the principal axis of anisotropic diffusion tensor of RRF molecule. The helices in domain I have amphiphilic properties and the constituting hydrophobic residues are positioned at the inner-face as usually seen in a helix bundle. Domain II, the foot portion of molecule corresponding to the horizontal line of L, of which instep is 30 Å long, is a three-layer β/α/β sandwich consisting of an α-helix (helix 2, residues 75-88), a two-stranded short antiparallel β-sheet (strand 1 and strand 2, residues 45-46 and 51-52) and a four-stranded antiparallel β-sheet (strand 3 and strand 4, residues 59-61 and 67-71; strand 5 and strand 6, residues 94-95 and 100-103). Strand 5 and strand 6 are connected by a β-turn. The toe of domain II is composed of the β-turn and two turns linking strand 1 and strand 2, and helix 2 and strand 4. The four-stranded antiparallel β-sheet has an amphiphilic profile and forms the hydrophobic core with helix 2. In the tri-peptide 37-39 region of domain II, backbone torsion angles show that these three residues are fit in a helical conformation, which coincide with the indication in the chemical shift data. This helical region was also indicated from the NMR analysis of *P. aeruginosa* RRF (*56*) and observed in the x-ray structure of *T. maritima* RRF (*15*).

Orientation of two domains. As shown in Figure 2-4b and 2-4c, the ensembles of structures were converged well individually. The average atomic root mean square deviation (rmsd) values for backbone atoms of both domains were 0.7 Å. On the other hand, the rmsd value for the whole molecule was substantially larger (1.4 Å). The relative orientation between two rigid bodies is given by the set of three spherical polar angles: Φ, ϑ, and X as shown in Figure 2-6. In this study, the z-axis of reference frame of domain I is defined by the long axis

of three-helix bundle, and its x-axis is set along the vector connecting the center of three-helix bundle to helix 1. On the other hand, the z'-axis of domain II is defined by the long axis of strand 5 and the x'-axis is set along the vector between strand 5 and helix 2. The average values of Φ, ϑ, and X , are 4.3°, 89.7° and –62.6°, respectively. The standard deviations of zenith angles, ϑ, and rotation angles of x'-axis around z'-axis, X, fall in narrow ranges (±4.5° and ±7.4°). But the standard deviation of azimuth angles, Φ, spans rather a wide range of ±17.4° .

Table 2-1: Structural statistics for the final structures of *A. aeolicus* RRF[a]

	rmsd from experimental restrains
distances (Å)	0.015 ± 0.003
torsion angles (deg)	0.81 ± 0.06
T_1/T_2 ratios	0.88 ± 0.09
	rmsd from idealized covalent geometry
bonds (Å)	0.0198 ± 0.0002
angles (deg)	0.42 ± 0.03
impropers (deg)	0.45 ± 0.04
	coordinate precision
domain I (residues 5-29, 109-142, 149-180)	0.68
domain II (residues 30-108)	0.73
whole molecule (residues 5-142, 149-181)	1.42

[a]The final force constants employed for the various terms in the target function used for structure calculation are as follows: 1000 kcal·mol^{-1}·Å^{-2} for bond lengths, 500 kcal·mol^{-1}·rad^{-2} for angles and improper torsions (which serve to maintain planarity and chirality), 4 kcal·mol^{-1}·Å^{-4} for the quartic van der Waals repulsion term, 30 kcal·mol^{-1}·Å^{-2} for the experimental distance restraints, 200 kcal·mol^{-1}·rad^{-2} for the torsion angle restraints, and 1.0 kcal·mol^{-1} for for the T_1/T_2 restraints. The precision of the atomic coordinates is defined as the backbone (C', Cα, N) rmsd between the 15 final structures and the mean coordinates. The disorderd residues 1-4, 143-148, and 181-184 are excluded for the calculation.

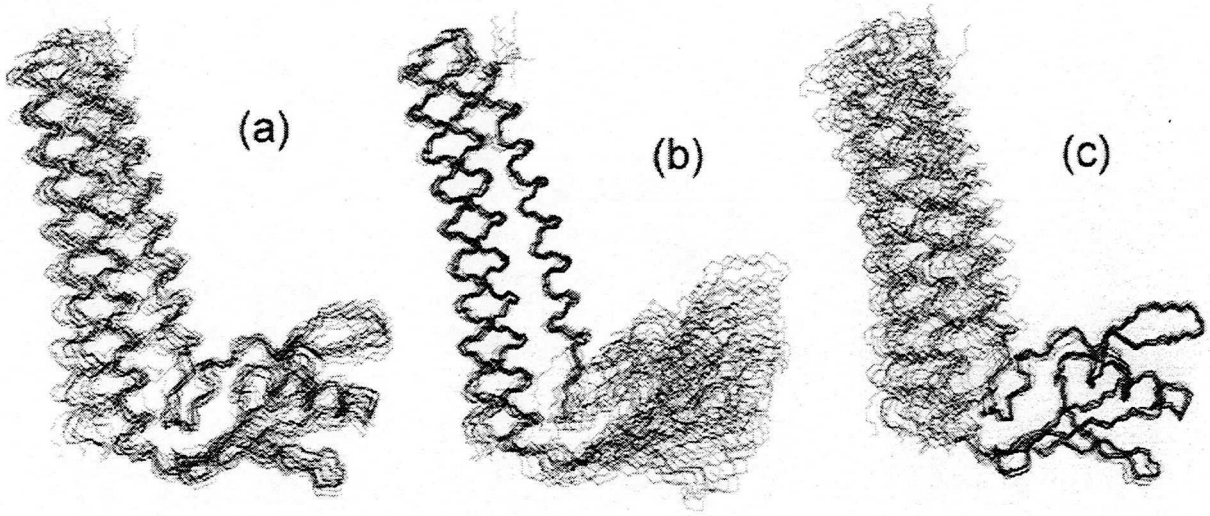

Figure 2-4. Best-fit superpositions of the backbone atoms of (a) whole molecule, (b) the domain I, and (c) the domain II of the 15 NMR-derived structures of A. aeolicus RRF. The rmsd values for backbone atoms of both domains were 0.7Å, indicating that the ensembles of structures converged well individually. On the other hand, the rmsd values for the whole molecule were substantially larger than 1.4 Å.

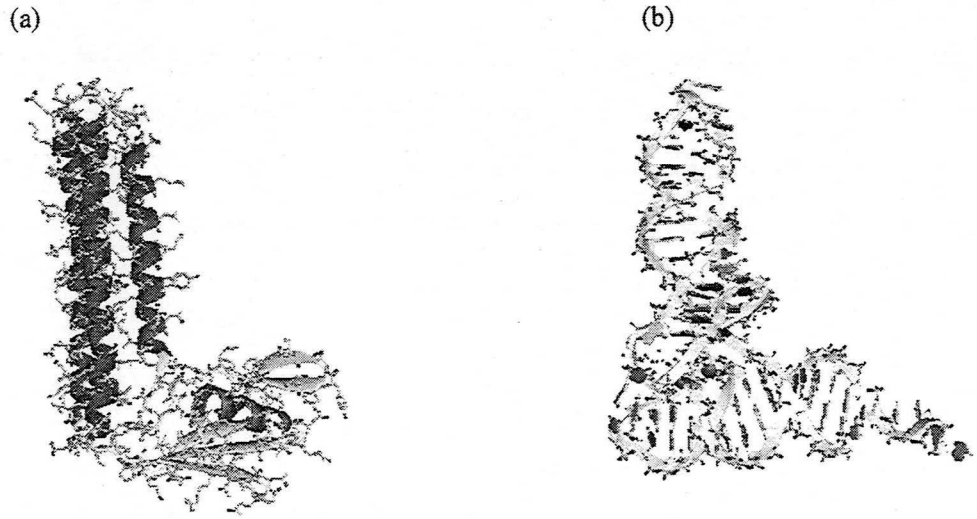

Figure 2-5. Schematic presentation of the structure of (a) *A. aeolicus* RRF, and (b) $tRNA^{Phe}$.

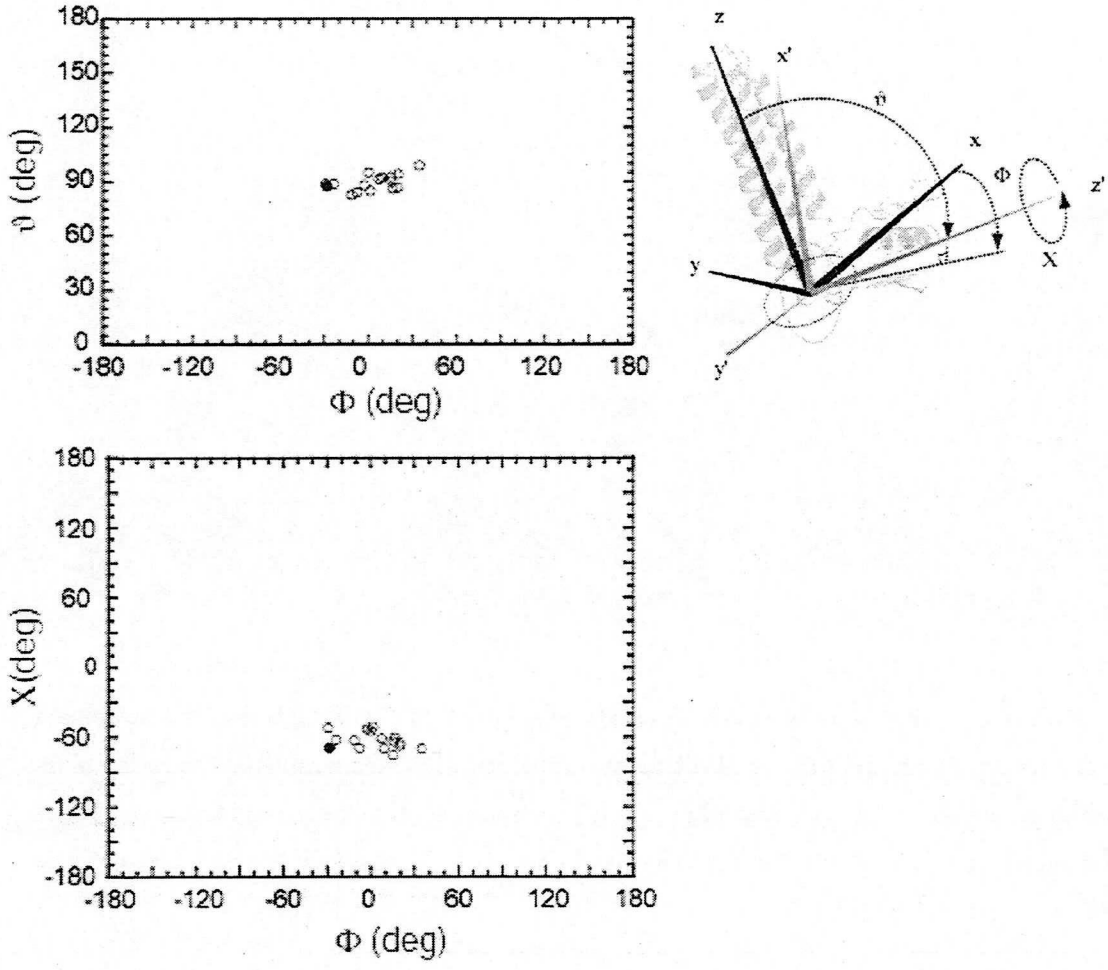

Figure 2-6. Distributions of interdomain angles for the ensemble of the 15 NMR-derived structures of *A. aeolicus* RRF (open circles), and for the x-ray structure of *T. maritima* RRF (closed circle). The interdomain angles are represented by the set of three spherical polar angles. The definitions for the angles are shown schematically (for detailed definitions, see the section of orientation of two domains in results). The average values of Φ, ϑ, and X are 4.3°, 89.7° and –62.6°, respectively. The standard deviations of Φ, ϑ and X are 17.4°, 4.5° and 7.4°, respectively.

Discussion

Recently, crystal structures of RRF from two different bacteria have been elucidated (*15, 16*). They are from hyperthermophilic bacterium, *Thermotoga maritima,* and from mesophilic bacterium, *Escherichia coli*. Both structures are almost similar to each other except for the angle between two domains and characterized by their overall profiles of an L-shaped conformation. The contact of the two domains is accompanied by an 8.2 % (981 $Å^2$) loss in

water-accessible surface area (*ASA*) in *T. maritima* RRF (*15*). As judged from the published results of *E. coli* RRF (*16*), loss in *ASA* due to domain contact is about the same or possibly even smaller than that of *T. maritima* RRF. These values are significantly smaller than those of usual domain interactions in which each domain forms stable binding to each other (*57*), suggesting weak interaction between the two domains of RRF molecule. Therefore, it is possible that packing forces or insertion of detergent molecule in the crystal is responsible for the difference between two structures of RRF.

The present result provides the structure of RRF in free state because *A. aeolicus* RRF was analyzed in solution free of crystal lattice restrains. Structure determination procedure by NMR usually relies on short range distance restraints. However, these restraints are not sufficient for the determination of the relative orientation of domains. The author have tried a couple of new methods, which have been recently developed for defining the long-range order in NMR structure determination (*58, 59*). These approaches utilize the information from the relaxation time dependence on rotational diffusion anisotropy or the residual dipolar coupling of weakly aligned molecules. In the present study, a well-converged structure could be elucidated through the relaxation time dependence approach. Figure 2-3 shows the agreement between the calculated and the observed ^{15}N T_1/T_2 ratios, which indicates that the T_1/T_2 anisotropy restraints are consistent with other restraints and reliable. Thus, the author could conclude that the characteristic tRNA like conformation of RRF molecule is maintained in solution. This supports the notion that RRF mimics the function of tRNA (*15*).

The structures for each domain of *A. aeolicus* RRF are basically in agreement with those of *T. maritima* RRF and *E.coli* RRF (*15, 16*). The backbone traces of domain I and domain II of *A. aeolicus* RRF can be superimposed on those of *T. maritima* RRF with rmsd values of 1.7 Å and 1.8 Å respectively. The *ASA* loss of *A. aeolicus* RRF accompanied by the domain-domain interaction is 829 $Å^2$ (6.5%), which is close to the value of *T. maritima* RRF (*15*). The small value in the *ASA* loss indicates that the two domains contact each other through a small area that seems to be insufficient to fix the structural arrangement between them. The intrinsic structure of the joint region, which is composed of double polypeptide chains (Leu30-Ser36 and Leu104-Thr108) with proline residues (Pro105, 106) that restrict the conformation of a polypeptide chain, may contribute to stabilize the tRNA like conformation of RRF in solution.

Regarding the relative orientations of two domains, differences among the three RRFs are found. The bending angle of the joint between the two domains (ϑ) in *A. aeolicus* RRF is 90° and seems to be significantly different from that of *E. coli* RRF (110°), but identical to *T. maritima* RRF (90°). As a result, *E. coli* RRF is an open L-shaped molecule rather than a strict L-shaped molecule. According to Kim et al. (*16*), this makes *E. coli* RRF not a near perfect mimic of tRNA in contrast to *T. maritima* RRF. The differences between *A. aeolicus* RRF and *T. maritima* RRF are found in the rotational direction of domain II around the long axis of domain I (Φ). The angle Φ varied 33±17° (error range is defined by the standard deviation) when domain I of each RRF was superimposed (Figure 2-6). These comparisons suggest that the rotational angle of domain II (Φ) can vary in solution while the angle between the domains (ϑ) may vary under the stress of crystal lattice formation. It is important to point out that the relative rotation of two domains appears to occur maintaining ϑ equal to 90° or without much of rotation of X. It is possible that the relative movement of these two domains is functionally important as discussed in a recent paper (*60*). As shown in Figure 2-6, fluctuations of the relative orientation between domain I and II are observed in the ensemble of NMR structures. Such disorder originates from a lack of structural restraints that may be due to internal mobility of the joint region. The values of ^{15}N-{^{1}H} *NOE* clearly show the flexibility of the joint region of *A. aeolicus* RRF (Figure 2-7). Recently, the activities of RRFs from several bacteria were investigated in *E. coli*. *P. aerginosa* RRF was shown to be active in *E. coli* (*61*) while *T. maritima* RRF is toxic to *E. coli*. Furthermore, *T. thermophils* RRF failed to complement the lethal mutation of *E. coli* on the RRF gene while truncated RRF could (*62*). The C-terminal truncation of *E. coli* RRF has also been shown to cause temperature sensitivity of the molecule (*4*) . These studies suggest that RRFs from thermophiles are able to bind to ribosome of *E. coli* but are inactive or less active in ribosome recycling assay performed at the room temperature. This is because RRFs from thermophiles were not endowed with the interdomain flexibility at the ambient temperature. Thus the author could conclude that the domain movement is important for its action against the ribosome.

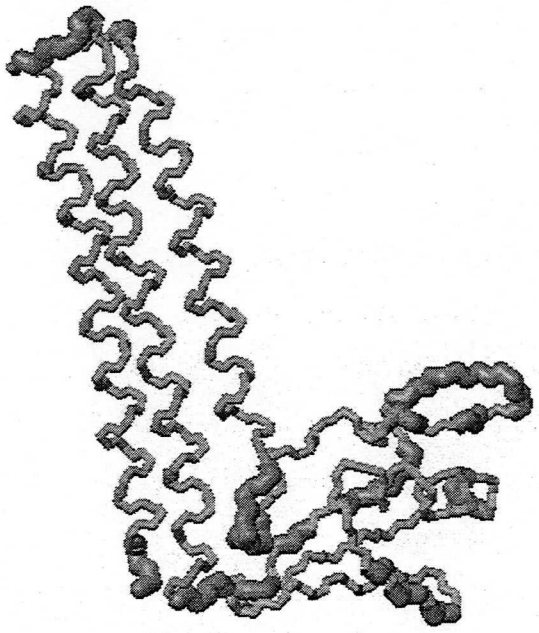

Figure 2-7. Rapid internal motion on the subnanosecond time scale for the backbone of *A. aeolicus* RRF. The trace is colored in red where the value of ^{15}N-{^{1}H} is smaller than 0.65.

Structures of domain I and domain II

The three-helix bundle structure found in *A. aeolicus* RRF is different from those of classical left-handed coiled-coils. The helices of *A. aeolicus* RRF are nearly straight and packed together with an unusual right-handed twist. In classical coiled-coils, the heptad repeats, $(abcdefg)_n$, which is a sevenfold repeat in the primary sequences, contribute to stabilize the left-handed supercoil through hydrophobic interactions at position "a" and "d" (*63*). As shown in Figure 2-8a, in the case of RRF domain I, the autocorrelation of hydrophobicity in the primary sequence reveals undecad (eleven fold) repeats of hydrophobic residues in addition to normal heptad. It is known that undecad repeats form a slightly right-handed supercoiled structure (*63*). Such mixture of heptad and undecad repeats may contribute to stabilize the characteristic straight three-helix bundle structure in RRF through hydrophobic interactions. The critical role of hydrophobic interactions at three-helix bundle on the stability is indicated in the study of temperature sensitive phenotype of *E.coli* RRF (*4*),

in which a single mutation (shown in Figure 2-8b) of a hydrophobic residue in domain I influences the thermal stability of RRF.

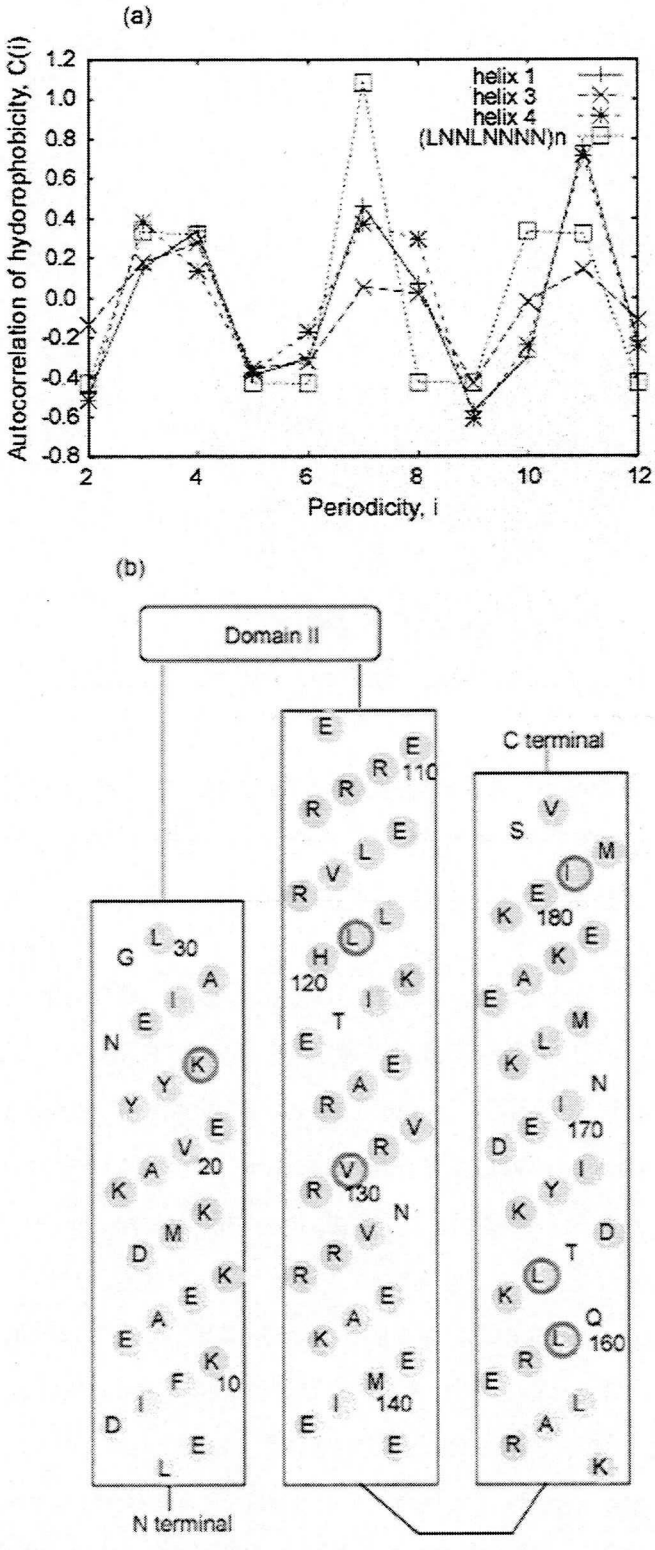

Figure 2-8. (a) Discrete autocorrelations, C(i), of hydrophobicity in the primary sequences (+; helix 1, ×; helix 2, and *; helix 4) of domain I of A.aeolicus RRF. The π values defined by

Fauchere and Pliska (*64*) are used as hydrophobicity. C(i) are calculated from a sum of $\pi(j)\pi(j+i)$, where j runs through the sequence. The values for the (Leu-Asn-Asn-Leu-Asn-Asn-Asn)n as a model of heptad repeats are also shown (open squares). (b) Schematic diagram of three-helix bundle of domain I. Residues consisting of hydrophobic core are placed in the center of each helix. Hydrophobic residues are filled in yellow. Residues with positive charges and negative charges are filled in blue and magenta, respectively. Red circles indicate the locations of substituted residues in temperature sensitive mutants of E. coli RRF (*4*).

Additionally, amino acid residues on the surface also modulate the stability of helices. Although no specific salt bridge (within 4.0 Å) was found in *A. aeolicus* RRF, the biased distribution of charged residues suggests that long-range electrostatic interactions may contribute to stability of RRF molecule. It has been reported that, compared to mesophiles, proteins of thermophiles show higher contents of charged amino acids (*65*), and that charged amino acids on surface of protein enhance thermostability (*66*). In case of thermophilic RRFs, the amount of charged residues (Asp, Glu, Arg, Lys and His) within the residues of three-helix bundle are larger (e.g. 52%; *A. aeolicus*, 52%; *T. maritima*) than that of mesophiles (e.g. 47%; *E.coli*, 44%; *P. aeruginosa*).

Domain I has a well conserved surface which is mainly composed of residues in helix 3. This region has a cluster of positive charges, which is effective for interacting with the negative charge of the phosphate backbone of RNA. Any mutation of Arg110, Arg129, and Arg132 of *E. coli* RRF (corresponding to Arg112, Arg131, and Arg134 of *A. aeolicus* RRF, respectively) is lethal (*67*). This experimental result supports the hypothesis that the surface of helix 3 might be necessary to interact with rRNA.

In contrast to the rigid structure of domain I, domain II has several flexible regions, which are reflected by low ^{15}N-{^{1}H} *NOE* values (Figure 2-7). These results are consistent with the notion that domain II is the basic structure critical for maintaining the function of RRF. It is therefore understandable that several lethal mutations (for example, Leu65Pro) but no temperature sensitive mutations were found in this domain (*67*). It is known that the flexible region of a protein is essential for its function (*68, 69*). It was noted that a conserved surface is located in the toe of domain II. This region consists of Tyr48, Trp73 and Asp74. These residues are unusually exposed to solvent and, therefore, may play a crucial role in recognition of the target molecule. Further investigation to identify the binding partner of RRF is in progress.

Chapter III

A Characteristic Domain Motion in the Ribosome Recycling Factor Revealed by ^{15}N NMR Relaxation Experiments and Molecular Dynamics Simulations

While a detailed mechanism of RRF action after the binding to ribosome is still unclear, a suggestive fact that RRFs from thermophilic bacteria are not comparable to *E. coli* RRF in the assay system containing *E. coli* ribosome and EF-G was shown by several experiments. Atarashi and Kaji suggested that the relative orientation of domains must vary during the reaction and that reduced flexibility of the hinge of RRFs from thermophilic bacteria at the ambient temperature is responsible for the inhibitory effect (*60*). Toyoda et al. examined whether the plasmid encoding mutant *T. thermophilus* RRF is able to rescue the RRF-knockout *E. coli* host. Interestingly, some mutants of *T. thermophilus* RRF, in which the flexibility of the hinge was enhanced, gained an activity in *E. coli* host cells (*17*). These results indicate that domain motion and/or plasticity for domain arrangement of RRF molecule is important for the activity of RRF. Therefore to understand the detailed mechanism of RRF action, it is important to establish a way to evaluate the dynamics in a RRF molecule. In fact, no direct evidence about domain motion of RRF in solution has been shown so far. To investigate dynamics of RRF, the author performed MD simulation and NMR relaxation analysis in this study.

Experimental Procedures

MD Simulations

The MD simulations were performed with GROMACS version 3.1 using GROMACS forcefield (*70, 71*). The protein molecule was solvated in a periodic box with the SPC water model (*72*). The clearance between the protein molecule and the edge of the box was at least 9 Å. A particle mesh Ewald method (*73*) was used to calculate electrostatic interactions, with a cut-off of 9 Å for the separation of the direct and reciprocal space summation. Van der Waals interactions were truncated at 9 Å. All chemical bonds were constrained using LINCS (*74*), allowing a time step of 2 fs for the integration of the equation of motion. During the MD run, the temperature was controlled using weak coupling (*75*) to a bath of constant

temperature and the pressure was controlled using weak coupling to a bath of constant pressure. The starting structure of MD for *E. coli* RRF was generated from the crystal structure of the Arg132Gly variant of *E.coli* RRF (*76*) (PDB: 1ISE) by restoring Gly132 to Arg. Since the reported X-ray structure of wild-type *E. coli* RRF (*16*) (PDB: 1EK8) is a complex with a detergent molecule, which affects the structure of domain II and the relative orientation of domains, the author used the detergent-free X-ray structure of the Arg132Gly variant of *E. coli* RRF instead. The initial part of simulation consisted of an energy minimization and 21 ps warming steps from 0.1 K to 303 K following an equilibration period of 47 ps at 303 K. At the end of this period, the total energy and the temperature were stable. From this point, coordinates were stored every 0.2 ps. The total length of MD run was 4.5 ns. The essential modes for collective motion (*77*) in a RRF molecule were analyzed using the covariance matrix M of the Cα coordinates x:

$$M_{ij} = \left\langle \left(x_i - \langle x_i \rangle\right)\left(x_j - \langle x_j \rangle\right) \right\rangle \qquad (1)$$

The covariance matrix was diagonalized to calculate the eigenvalues and eigenvectors. The principal mode corresponding to the largest eigenvalue describes the representative collective motion. To demonstrate the range and the direction of that motion, the two extreme projections on the average structure were calculated.

The autocorrelation function C(t) for internal motion of the N-H bond vectors was calculated by :

$$C(t) = \langle P_2(\mu(0)\mu(t)) \rangle = \sum_{i=1}^{N} P_2(\mu(\tau_i)\mu(t+\tau_i)) \qquad (2)$$

where μ(t) is the N-H unit vector at time t, and N is the number of data points used for averaging, and P_2 is the second-rank Legendre polynomial. Coordinates snapshots were superimposed onto the starting structure of MD run by using the backbone atoms to remove the overall motion. The generalized order parameter is defined by a plateau value of the autocorrelation function (*78, 79*). Although the autocorrelation functions did not converge in the MD run of RRF, a typical autocorrelation function immediately dropped below 1.0 after several picoseconds and then gradually decreased. Thus, the author estimated the order parameter for fast motion from

$$S_f^2 = \frac{1}{\Delta T} \int_{T}^{T+\Delta T} C(t)dt \qquad (3)$$

where T=10 ps and ΔT=10 ps.

NMR Experiments

E. coli RRF was expressed using pET system (Novagen, Madison, WI) in *E. coli* strain BL21(DE3). Uniformly ^{15}N-labeled protein was obtained by growing cells in M9 medium containing $^{15}NH_4Cl$ as the sole nitrogen source. *E. coli* RRF was purified as described by Kim et al (*16*). The NMR samples of RRFs were prepared in 90% H_2O/10% D_2O HEPES buffer of 10 mM at pH 7.4 with 50mM NaCl. A protein concentration of 0.5 mM was used for NMR measurements.

NMR measurements were performed on a Varian INOVA600 spectrometer. Transmitter frequencies for ^1H and ^{15}N were 4.76 and 119.0 ppm, respectively. The backbone ^{15}N relaxation parameters, T_1, T_2, and ^{15}N-{^1H} *NOE* were measured using HSQC type pulse sequences (*39, 80, 81*). The T_1 relaxation decay was sampled at six time points (30, 108, 204, 420, 720, and 1050 ms). The T_2 relaxation was measured both by using a ^{15}N spin-locking sequence with a field strength of 2.4 kHz and by using a CPMG-type sequence. The T_2 decay was sampled at six time points (12, 24, 36, 48, 60, and 72 ms). The T_2 values measured using spin-locking were calculated from the decay constant, $T_{1\rho}$, and the T_1 with the resonance offset frequencies and the strength of the spin-lock field. The ^{15}N-{^1H} *NOE* values were derived from two series of spectra, recorded with and without 3.5 s of saturation of the amide protons, respectively. The delay times between scans were about four times the nonselective T_1 value for ^1HN. In order to minimize the effects of spectrometer drift during experiments, all data were measured in an interleaved manner. All experiments were performed twice to check experimental reproducibility. Data were processed using the NmrPipe (*26*) and spectra were analyzed using PIPP (*27*) and in-house written programs. The T_1 and $T_{1\rho}$ values were obtained by nonlinear least-squares fitting of a two-parameter monoexponential function through the peak intensities. Errors in the derived relaxation times were estimated by Monte-Carlo type procedures. Resonance assignments were taken from our previously reported results (*82*). Residues undergoing chemical exchange were characterized by variation of values of $T_{2,\text{spinlock}}$ / $T_{2,\text{CPMG}}$ and values of $[(\langle T_2\rangle - T_2)/\langle T_2\rangle]-[(\langle T_1\rangle - T_1)/\langle T_1\rangle]$ (*83*). In the case of *E. coli* RRF, because both values of each residue were within the range of 1.5 times standard deviation from their mean values in the molecule, chemical exchange contribution to T_2 relaxation was ignored in the following analyses.

Model-Free Analysis

The measured relaxation parameters, T_1, T_2, and ^{15}N-{^{1}H} *NOE*, are related to the spectral densities by following equations (*84*):

$$
\begin{aligned}
1/T_1 &= (d^2/4)[J(\varpi_H - \varpi_N) + 3J(\varpi_N) + 6J(\varpi_H + \varpi_N)] + c^2 J(\varpi_N) \\
1/T_2 &= (d^2/8)[4J(0) + J(\varpi_H - \varpi_N) + 3J(\varpi_N) + 6J(\varpi_H) + 6J(\varpi_H + \varpi_N)] \\
&+ (c^2/6)[3J(\varpi_N) + 4J(0)] \\
NOE &= 1 + (d^2/4)(\gamma_H/\gamma_N)[6J(\varpi_H + \varpi_N) - J(\varpi_H - \varpi_N)]T_1
\end{aligned}
\qquad (4)
$$

where $d=[\mu_0 h\gamma_N\gamma_H/(8\pi^2)]\langle 1/r^3_{NH}\rangle$, $c^2=(\omega_N^2/3)(\Delta\sigma)^2$, ω_N and ω_H are the Lamor frequencies of the ^{15}N and ^{1}H nuclei, respectively, μ_0 is the permeability of free space, γ_N and γ_H are the gyromagnetic ratios of ^{15}N and ^{1}H, h is Planck's constant, r_{NH} is the length of the amide bond, and $\Delta\sigma$ is ^{15}N CSA value, which is the difference between parallel and perpendicular components of the ^{15}N chemical shift tensor. The value of -172 ppm was used as ^{15}N CSA (*85*).

Because the RRF molecule has a very anisotropic shape, spectral densities should depend on the orientation of the N-H inter-nuclear vectors and on their fluctuations relative to the diffusion tensor. In the case of an axially symmetric diffusion tensor ($D_{xx} = D_{yy}$), the model-free spectral density function (*78, 79*) at a frequency ω is approximated by

$$
J(\varpi) = \frac{2}{5}\sum_{j=1}^{3} A_j \left[\frac{S^2\tau_j}{1+(\varpi\tau_j)^2} + \frac{(1-S^2)\tau_j^e}{1+(\varpi\tau_j^e)^2} \right] \qquad (5)
$$

with:

$$
A_1 = 0.75\sin^4\alpha, A_2 = 3\sin^2\alpha\cos^2\alpha, A_3 = (1.5\cos^2\alpha - 0.5)^2
$$

$$
\tau_1 = (4D_{zz} + 2D_{xx})^{-1}, \tau_2 = (D_{zz} + 5D_{xx})^{-1}, \tau_3 = (6D_{xx})^{-1}
$$

where α is the angle between the principal axis of the axially symmetrical diffusion tensor and the N-H vector.

To test the validity of simple model-free analysis on the internal motion and the rotational diffusion property of RRF, experimental relaxation data for residues were fitted with the model function (5) by using the program Model-Free (*86*). In this analysis, the data for residues in well-defined secondary structure were used for fitting with an axially symmetrical diffusion tensor. Relative orientations of N-H bond vectors were obtained from the crystal structure. To take into account the possibility that the relative orientation of domains in the crystal differ from that in solution, each domain was rotated to align its principal axis of the diffusion tensor to z-axis before the calculation for the whole molecule.

Extended Model-Free Analysis for Domain motion

To evaluate the rigid body motion for each domain, observed relaxation data were fitted with the model function

$$J(\varpi) = \frac{2}{5}\sum_{j=1}^{5} A_j \left[\frac{S_f^2 S_s^2 \tau_j}{1+(\varpi\tau_j)^2} + \frac{S_f^2(1-S_s^2)\tau_j^s}{1+(\varpi\tau_j^s)^2} + \frac{(1-S_f^2)\tau_j^f}{1+(\varpi\tau_j^s)^2} \right] \qquad (6)$$

with:

$1/\tau_j^i = 1/\tau_j + 1/\tau_i$ where i = s or f.

This function has the same form as the extended model-free spectral density function in which the slow and fast motions have different correlation times (τ_s, τ_f) and order parameters (S_f, S_s). Clore et al. introduced this function for analyzing local slow motion in flexible region of a protein (*87*). In the present analysis, the author applied the function for analyzing the collective motion of each domain. For this purpose, τ_s was forced to be uniform for each domain. To take account of anisotropy of domain motion, the order parameter for the motion on a slow time scale, S_s, was optimized for each residue. The order parameter for fast local motion, S_f, was fixed at the value obtained from the MD trajectory. The correlation time for fast local motion, τ_f, was approximated to be zero. In this model, the author assumes that each domain moves in a molecular frame that tumbles in solution and that the domain motion is decoupled from the rotational diffusion of the molecule. Therefore, the rotational diffusion tensor was optimized globally for a molecule. ^{15}N T_1, T_2 and ^{15}N-{^{1}H} *NOE* data were fitted simultaneously on the basis of the atomic coordinates optimizing parameters described above. In this procedure, the average orientation of the long axis of the rotational diffusion tensor relative to the coordinates of each domain was also optimized. In consideration of the results of MD, where each domain of RRF molecule diffuses within a limited range, that value was restricted within the range sampled in MD trajectory. The author found, however, that the relative orientation of each domain has little effect on calculated order parameters (data not shown). All calculations were done with an in-house written program. Similar applications of the extended model-free spectral density function were recently reported (*88, 89*).

RESULTS

MD Simulations. To analyze the domain structure of the RRF molecule, a distance fluctuation map (DFM) (*90*) was calculated. The DFM revealed characteristic domain structure of RRF molecule as shown in Figure 3-1. The triangles and rectangle in DFM demonstrate that the

distance fluctuations inside each domain are smaller than those between domains. In other words, the author have confirmed the composition of domain structure from a dynamic point of view. Essential dynamics analysis using the covariance matrix revealed domain motion. As shown in Figure 3-2a, a dominant collective motion corresponding the largest eigenvalue exists in the RRF molecule. This motion is variation of the relative arrangement of domains (Figure 3-2b, 3-2c). Characteristic dynamics were also found in rms deviations (RMSD) of Cα coordinates during simulation from mean structure as shown in Figure 3-3. When only domain I is used for superposition in calculation of RMSD, the RMSD value for domain II is significantly larger (0.5 Å on average) than that for domain I (0.1 Å) and vice versa. Interestingly, the time evolutions of RMSD show an oscillation from 0.2 Å to 1.0 Å on a nanosecond time scale.

Figure 3-4 shows typical profiles of correlation functions for internal motion of N-H vectors obtained from MD trajectory. An initial drop during the first a few picoseconds is observed for all residues. After this burst phase, most of the correlation functions of residues in domain I decrease very slowly. However, correlation functions of many residues in domain II show more complex behavior. Several residues indicate oscillation of correlation functions. The order parameters for fast local motion, S_f^2, which were estimated from equation (3), are presented in Figure 3-5. S_f^2 has a quite uniform value of about 0.87 in the α helix region. In the β sheet region, S_f^2 values are distributed in a range between 0.75 and 0.85. In the peptide segments between regular secondary structures, most of S_f^2 values are lower than 0.7.

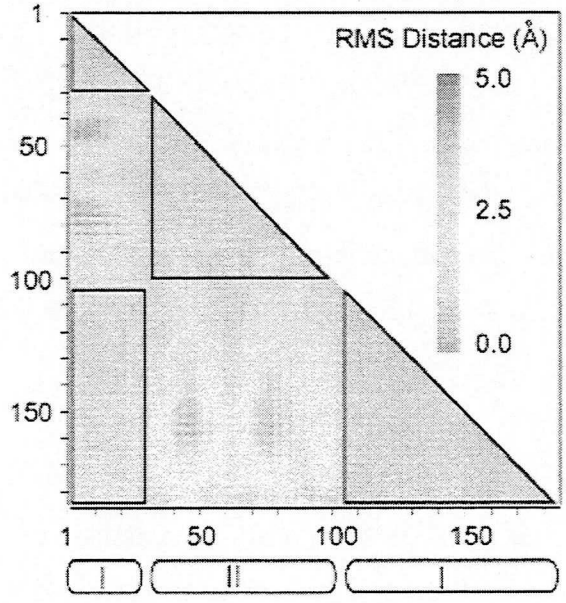

Figure 3-1. Distance fluctuation maps (DFM) calculated from 4.5 ns MD trajectories for *E. coli* RRF. DFM represents the fluctuation of distances between two Cα atoms, R_{ij}.

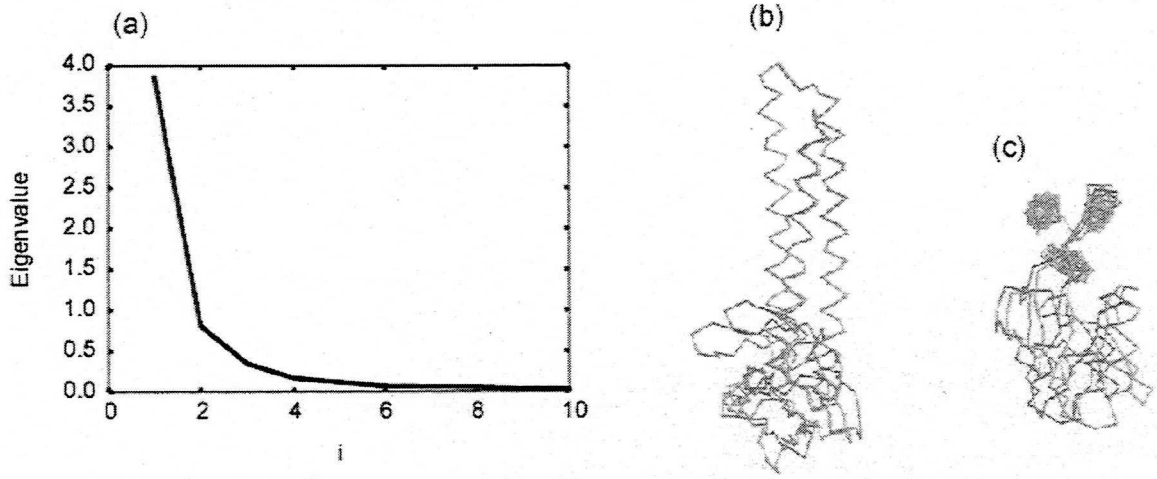

Figure 3-2. Essential dynamics analysis for 4.5 ns MD trajectories of E. coli RRF. (a) First 10 eigenvalues. (b, c) The two extreme projections for the motion corresponding to the largest eigenvalue are superimposed for the best fit over domain I.

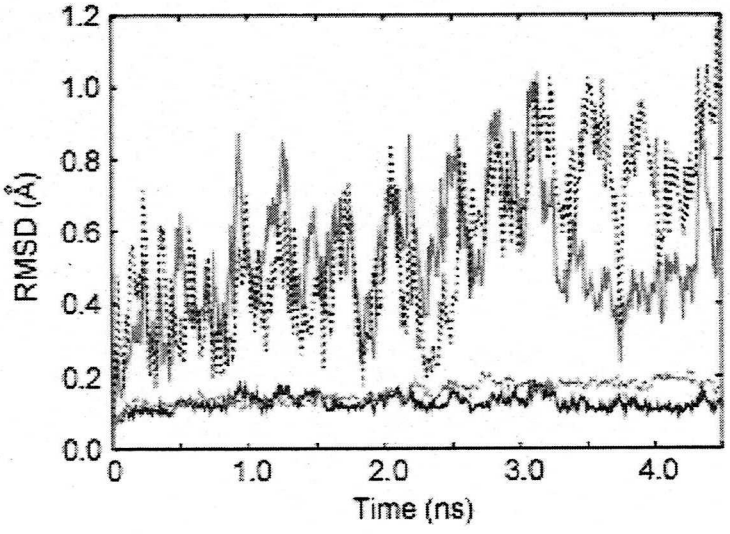

Figure 3-3. Time evolution of Cα root mean square deviations (RMSDs) with respect to the initial structure. RMSD of domain I superimposed for the best fit over itself (solid blue line), RMSD of domain I superimposed for the best fit over domain II (dashed blue line), RMSD of domain II superimposed for the best fit over domain I (solid red line), and RMSD of domain II superimposed for the best fit over itself (dashed red line).

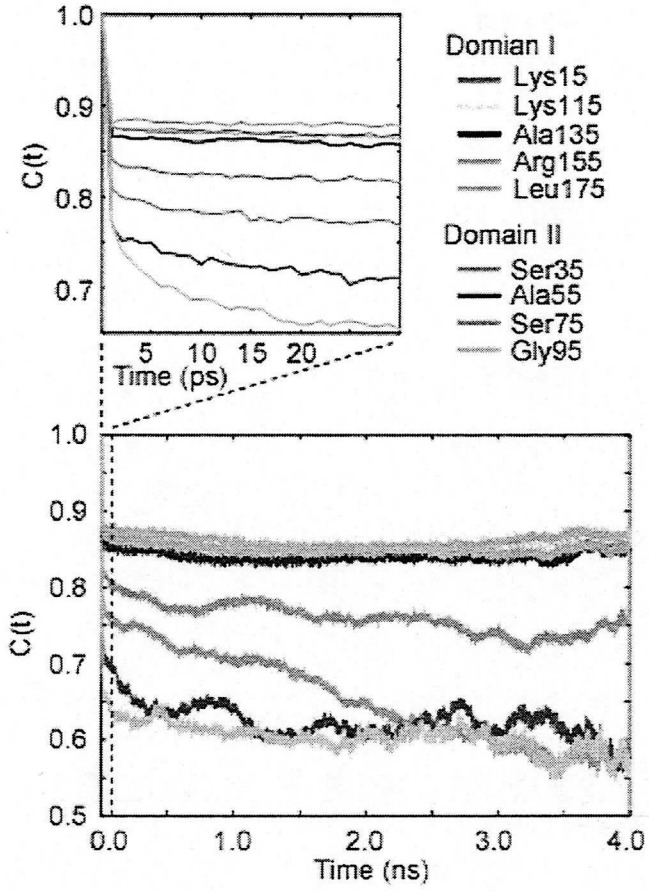

Figure 3-4. Correlation functions for internal motion of NH vectors of several residues calculated from 1.5ns MD trajectory.

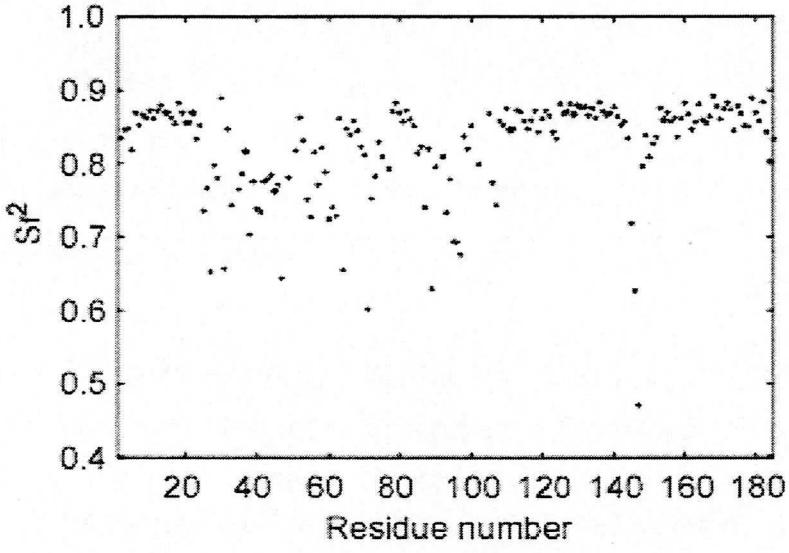

Figure 3-5. Order parameters for fast internal motion calculated from MD trajectories of *E. coli* RRF. Values were obtained from the correlation functions at 15 ps.

NMR relaxation measurements. Almost all resonances expected to give peaks in ^{1}H-^{15}N HSQC spectra were observed. However, very weak or overlapping resonances are difficult to quantify for spin relaxation measurements. Among 185 residues, T_1, T_2, and ^{15}N-{^{1}H} *NOE* values from 140 residues for *E. coli* RRF were obtained. The relaxation measurements were repeated twice, and the pairwise rms differences were 5 % for T_1, 3 % for T_2, and 5 % for *NOE*. The analyzed T_1, T_2, and ^{15}N-{^{1}H} *NOE* values are presented in Figure 3-6. The distribution of these values clearly shows a bimodal profile, which is similar to that observed in the case of *A. aeolicus* RRF (*91*) Such profiles indicate that *E. coli* RRF has a characteristic two domain structure in solution.

Relaxation analysis. The results of simple model free analyses are shown in Table 3-1. The large values of the mean squared errors for whole molecule show that the quality of fit in simple model-free approach is poor. The averaged values of calculated order parameters are significantly larger than the normal value obtained in the well-defined region of protein, which is generally about 0.85. Furthermore, the experimental correlation times for local motion, τ, are slightly larger than the expected value for fast librational motion. Such results suggest that some motion exists that has not been considered in the simple model-free approach.

The effective correlation times for domain I and domain II are 18.6 ns and 13.8 ns, respectively. The ratio between these values is 1.35. The deviation from unity suggests that these domains do not tumble as a rigid entity and that nanosecond ordered domain motions are present. Therefore, the author applied the extended spectral density function to account for such motion. The results of such analyses are shown in Table 3-2 and Figure 3-7. It is noteworthy that the value of the mean squared errors substantially decrease in this model as compared with that in simple model-free analyses. A small residual indicates the extended model is more meaningful. The overall correlation time is 21.8 ns while internal motions of domains on a time scale of 2 ns were obtained. The optimized order parameters (S_s^2) in domain I and domain II of *E. coli* RRF are distributed in the ranges of 0.89±0.03 and 0.73±0.07, respectively.

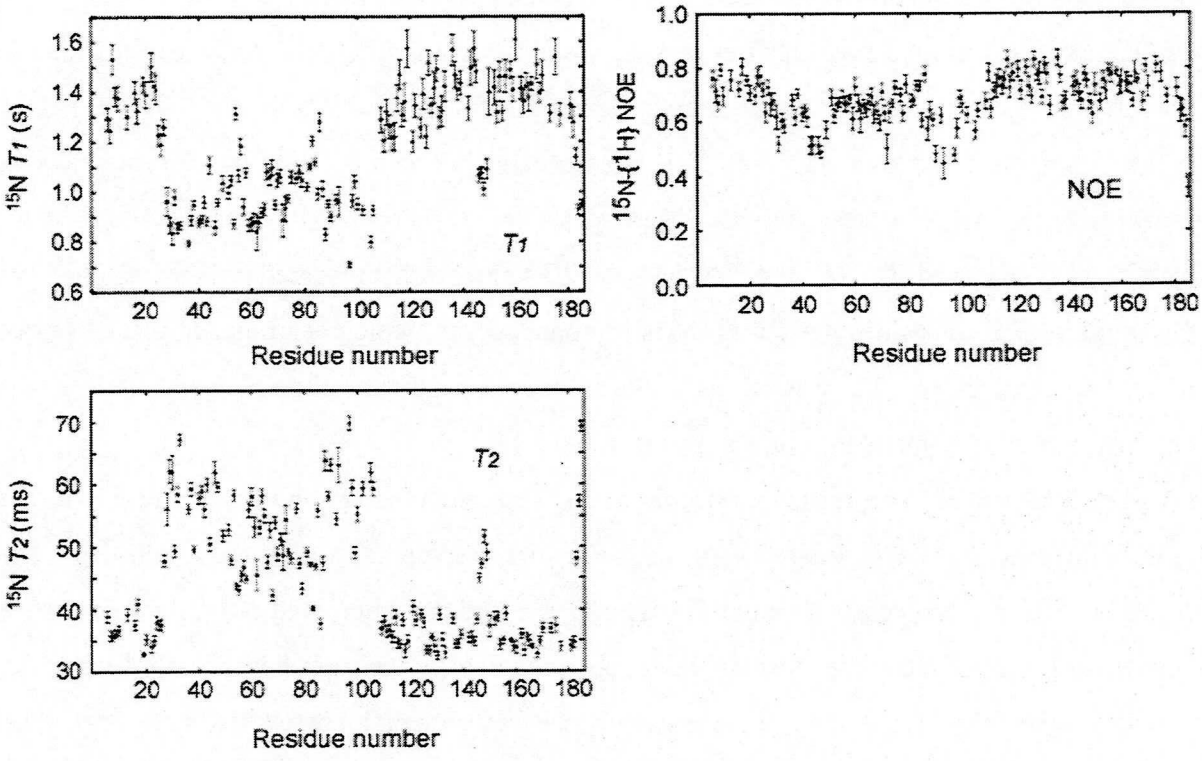

Figure 3-6. ^{15}N relaxation data at 30 °C and at ^{1}H frequency of 600 MHz for *E. coli* RRF. Error bars indicate standard deviations of data obtained by least squares.

Table 3-1. Results of simple model free analysis for ^{15}N relaxation data of RRF.

domain	$\tau_{c,eff}$(ns)	A	$\langle S^2 \rangle$	$\langle \tau \rangle$(ps)	MSE[a]
I	18.6	1.47	0.94	142	9.0
II	13.8	1.89	0.90	444	14.7
all	14.8	2.40	0.92	168	16.4

[a] mean squared error defined by χ^2 divided by the degree of freedom of fitting.

Table 3-2. Results of extended model free analysis for ^{15}N relaxation data of RRF.

domain	$\tau_{c,eff}$(ns)	A	$\langle S_s^2 \rangle$	τ_s(ns)	MSE[a]
I	-	-	0.89	2.1	-
II	-	-	0.73	1.9	-
all	21.8	1.81	-	-	7.4

[a] mean squared error defined by χ^2 divided by the degree of freedom of fitting.

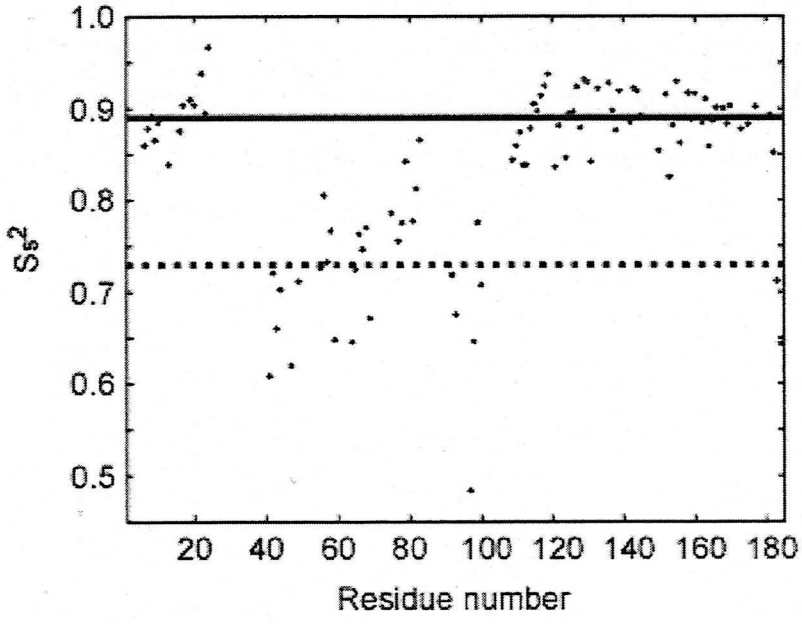

Figure 3-7. Order parameters for slow domain motion (S_s^2) obtained from extended model free calculation. Solid line and dashed line represent 0.89 and 0.73, which are the mean values of S_s^2 for domain I and domain II, respectively. The outliers, Asp97, Met183, and Gln184, are excluded for calculation of the mean values.

DISCUSSION

Although the importance of ribosome recycling step for cell viability and an essential role of RRF in that step have been reported earlier, the detailed mechanism of the ribosome recycling process by RRF has not been established. Recently, the importance of the fluctuation in inter-domain orientation was suggested from some genetic experiments (*17, 60*). In this study, a characterization and a quantification of internal motion of RRF molecule are presented.

The structure of RRF is structurally divided into two domains. As shown in Figure 3-3, the RMSD value for each domain is about 0.1 Å during MD simulation. This result supports the likelihood that each structural domain of RRF behaves as a rigid body. On the other hand, the spatial arrangement of the domains varies on a nanosecond time scale. The essential dynamics analysis shows that each domain undergoes a dominant collective motion. As shown in Figure 3-2, this motion can be described as a limited rotation of domain II, approximately 11°, around the bundle axis of domain I. In that motion, the characteristic L-shape structure of RRF as a mimic of tRNA is maintained. This nature of dynamics in the RRF molecule had been suggested by a comparison of crystal structures (*17*) with the NMR determined structure ensemble (*91*). Because the length of MD simulation was limited to 4.5 ns, the rare events that change domain orientation significantly may not have been sampled. Thus, the range of domain motion in MD simulation corresponds to the lower limit.

The simple model free analysis of ^{15}N relaxation data, where domain fluctuation was not considered, gave poor quality of fit. In that analysis, the calculated order parameters may be overestimated. That anomaly could be explained as follows. In the procedure of the simple model free analysis, T_1/T_2 ratio, which is not influenced by fast internal motion, is used to estimate overall correlation time (τ_c). However, T_1/T_2 is actually reduced when a significant slow global motion exists. In such a case, τ_c is underestimated. The order parameter calculated by the simple model free analysis corresponds to the ratio of the experimentally obtained spectral density to the estimated τ_c at zero frequency. As a result, the order parameter is overestimated when a slow global motion exists. In general, such an effect should be considered when dynamics of a multi domain protein is analyzed by the simple model free approach.

The ratio of τ_cs between domain I and domain II, 1.35, indicates that domain I is more restricted spatially than domain II, although it is difficult to quantify the mobility in relative

orientation of domains by the simple model free analysis. Then, the author attempted to interpret experimental data using an extended model free spectral density function. Although similar applications of that function for analyzing slow inter-domain motion of Ca^{2+}-ligated calmodulin and FBP3/4-M29 complex using multiple field experiments were recently reported (*88, 89*), our approach is somewhat different from theirs. The author employed an approach where MD simulation was used to complement NMR experiments at a single field. As mentioned in the literature, the analysis of relaxation data measured at multiple fields is very useful to detect such a slow global motion in multi domain protein and is superior in the point that it requires experimental data only without any a priori assumptions for parameters. However, NMR experiments at multiple fields also present some difficulties. At high field, the contribution of chemical exchange and variations in chemical shift anisotropy are increased. At low field, resolution and sensitivity become problems for large proteins. Indeed, when the author tried to obtain a set of NMR data at 500 MHz of ^1H frequency, a severe spectral overlapping made a quantitative analysis difficult. From the analysis of MD trajectory, order parameters for local fast motion (S_f^2) can be derived (*92*). Thus, from relaxation data at a single field the author could reduce the number of variables so as to determine parameters for both rotational diffusion of the molecule and domain motion. Off course, our method and reported ones are not exclusive. The combination and comparison of both approaches might provide further insights into domain motion of proteins and are in progress. Furthermore, instead of optimizing the order parameter for the motion on a slow time scale, S_s, per domain, the author optimized that value per residue. The structures of two domains of RRF are not similar each other and the relative rotation of domains is allowed within a limited direction. These are properties different from those of dumbbell-like molecules in which the applications of extended model free analysis have been reported (*88, 89*). In the case of RRF, each residue would not experience a unique motion even in a domain. Therefore, the author assigned a S_s value per residue.

The mean value of order parameter for slow domain motion (S_s^2) in domain I of *E. coli* RRF was 0.89±0.03. This value indicates that domain I of RRF molecule is nearly fixed on the diffusion frame of the molecule. On the other hand, the mean value of S_s^2 in domain II was 0.73±0.07 and indicates that domain II of RRF is more flexible than domain I. Considering that each domain would diffuse in a cone of semi-angle θ, the observed order parameters correspond to a θ of 16° for domain I and to a θ of 26° for domain II. Interestingly, in

domain II , S_s^2 values of the α helix are relatively larger (0.80±0.04) than those of β sheet region (0.71±0.05). There are two possible reasons for the variety of S_s^2 values within the same domain. One is that the internal motion in domain II occurs on a medium time scale. When such motion exists, the domain motion may be overestimated. Another possibility is that the variations in calculated S_s^2 values in a domain indicate that the motion of each domain is anisotropic, not isotropic free diffusion. Such anisotropic domain motion has been indicated in the analysis of MD simulation. Modulation of spectral density function by anisotropic motion is dependent on the averaged orientation of inter nuclear vector. Therefore, the analyses of the correlation between S_s^2 values and the orientation of inter nuclear vector should provide information about anisotropy of domain motion, e.g. the axis of rotation. Actually, the author could not detect such correlations. Because the N-H inter-nuclear vectors distribute within a narrow range in three helix bundle of domain I and in β sheets of domain II, the directional information may be insufficient to obtain such correlations. The analyses on relaxation of other nuclei which sample a different direction, e.g. $^{13}C\alpha$ and $^{13}C'$, may help for solving this problem and are in progress.

The goal of this work is to clarify the contribution of internal motion and/or plasticity of RRF to the ribosome recycling process. The author has demonstrated that the combination of MD calculation and NMR relaxation analysis is a powerful strategy for analyzing intra-molecular dynamics of RRF. In this study, the MD simulation has revealed that each domain of RRF molecule undergoes a collective motion. The variation of relative arrangement between domains is described as a limited rotation around a hinge axis, which is nearly parallel to the bundle axis of domain I. The tRNA mimicking L-shape of RRF was shown to be maintained during such rotation. This NMR study demonstrates that the range of rotation of domain II in solution is about 30° as a cone semi-angle. These results indicate that the joint regions between the domains are flexible and relative arrangement of the domains can be easily changed in a certain direction by an external force. The characteristic dynamics of RRF molecule may be attributed to the geometry of peptide chains in joint regions, which is presented in Figure 3-8. Because the two peptide chains of joint regions are arranged nearly vertically about the bundle axis of domain I like two hinges of a door, the bending angle between domains is maintained at a right angle. But domain II is able to flap by swinging around the bundle axis of domain I. As the amino acid sequence of joint regions are well conserved in RRFs (*17*), the characteristic dynamics of RRF molecule is likely to be

conserved evolutionally to contribute to its activity. Recently, the author proposed a model for the binding mode of RRF to ribosome where domain I is bound to the 50S subunit and domain II does not participate in ribosome binding at the A-site (*19*). In that model, domain II is able to change its position toward the P-site as mentioned above. The conformational change of EF-G upon GTP hydrolysis could be transmitted through this movement of domain II to the P-site bound tRNA, consequently RRF may help release tRNA thereby resulting in ribosome recycling reaction.

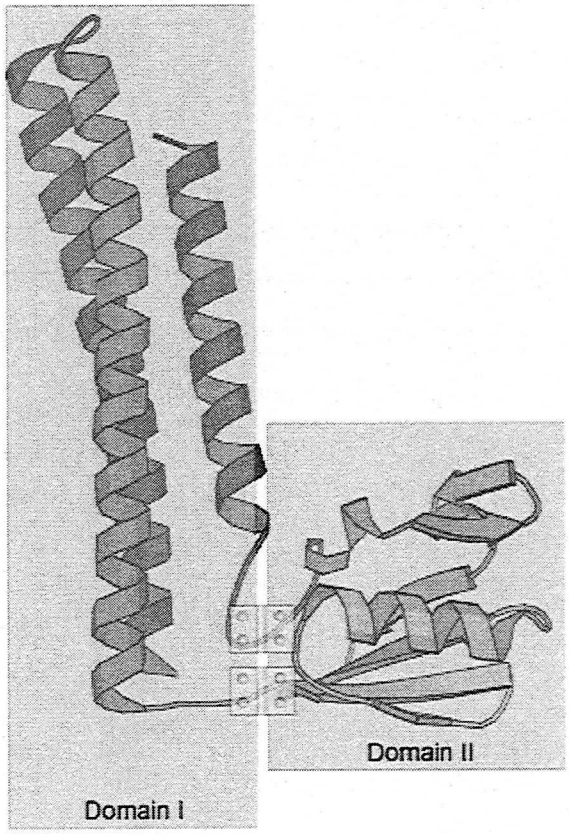

Figure 3-8. Spatial arrangement of two peptide chains of the joint region between domains I and II as modeled by a swinging door.

Concluding Remarks

In this study, the author extensively analyzed the structure and dynamics of ribosome recycling factor by means of NMR spectroscopy. The findings in this study would provide a deeper insight of the mechanism of ribosome recycling.

First, the author established the NMR assignments of RRFs originated from five bacteria. Resulting assignments bring not only the basis of following structural study, but also the set of interaction probes at an atomic resolution. As indicated by Fesik et al. (*93*), binding analysis using NMR spectroscopy is particularly fruitful in target-directed drug discovery. Because RRF is essential for bacterial life, but not for eukaryotic cells, RRF could be an ideal target for novel therapeutic antimicrobial agent. The author is now carrying a screening study for RRF inhibitor by NMR spectroscopy.

Second, the author was interested in structure determination of RRF in solution. The resulting structure of *A. aeolicus* RRF has an tRNA-like L-shaped conformation with two domains. Domain I corresponding to the vertical line of L, is a characteristic three α–helix bundle. Domain II corresponding to the horizontal line of L, has α/β/α sandwich structure. This result strongly supports that the L-shaped conformation is an intrinsic property of RRF molecule and an open L-shaped conformation observed in the crystal structure of *E. coli* RRF is artifact. The analysis of inter-domain orientation in the ensemble of calculated NMR structures suggested that azimuth angle of domains is variable within a limited range. The structural information of the RRF molecules in solution should provide a clue to understanding the ribosome recycling and further knowledge about the translation process on the ribosome of a prokaryote. One of our goals is to design rationally an antibiotic as a specific inhibitor for the RRF molecule using this information.

Finally, the author investigated inter-molecular dynamics of RRF by NMR relaxation analyses and nanosecond molecular dynamics simulations. The results revealed characteristic flexibility in inter-domain orientation of RRF molecule experimentally, which has been indicated in structural study.

Recently the author and colleagues constructed a RRF-ribosome complex model based on an interaction study using biacore and filter techniques (*19*). In the model, domain II of RRF would face the ribosomal P-site and the factor binding site where EF-G is bound. As shown in chapter 2, a hydrophobic patch is located on the tip of domain II. The tip region of domain

II may play a crucial role in recognition of the target molecule. The significance of the interactions of RRF with EF-G has been reported based on the fact that *Mycobacterium tuberculosis* RRF is inactive in *E. coli*, but it regains activity upon co-expression of *M. tuberculosis* EF-G (*94*). From the mutational studies of RRF and EF-G, Ito et al. have proposed that EF-G motor action is transmitted to RRF (*95*). As described in chapter 3, azimuth angles between domains can vary in the range of approximately 50°. Such a domain movement or conformational change may occur upon EF-G binding. It has been proposed as a hypothetical mechanism that RRF may be bound first to the A-site of the ribosome and then translocated by EF-G to the P-site in a manner similar to that of tRNA, leading to the disassembly of the post-termination complex (*15*). The author and colleagues examined whether the mechanism is consistent with the RRF-ribosome complex model. Joseph and Noller reported that the anticodon stem loop of tRNA is required in the A-site for translocation by EF-G during the elongation step (*96*). However in our model, RRF lacks the part corresponding to the anticodon stem loop of tRNA. Therefore RRF is not likely to be translocated from the A-site to the P-site by EF-G. Furthermore it was shown that the release of tRNA from post-termination complex partially takes place with EF-G alone (*97*). Therefore, we propose that RRF does not go through a translocation from the A-site to the P-site with the help of EF-G. In this respect, RRF is not a perfect functional tRNA mimic. Movement toward the P-site or conformational change of domain II might assist tRNA release from post-termination complex by EF-G, while domain I still keeps the A-site occupied to protect the A-site against the incoming EF-Tu-aminoacyl-tRNA complex during the disassembly reaction. The author have pointed out that movement of the Φ angle that maintains the L-shaped structure is important for RRF action. Based on this view, the physicochemical study to elucidate the differnce in RRF actitvity between mesophilic and thermophilic bacteria is in progress.

REFERENCES

1. Hirashima, A., and Kaji, A. (1970) *Biochem Biophys Res Commun 41*, 877-83.
2. Janosi, L., Shimizu, I., and Kaji, A. (1994) *Proc Natl Acad Sci U S A 91*, 4249-53.
3. Ryoji, M., Berland, R., and Kaji, A. (1981) *Proc Natl Acad Sci U S A 78*, 5973-7.
4. Janosi, L., Mottagui-Tabar, S., Isaksson, L. A., Sekine, Y., Ohtsubo, E., Zhang, S., Goon, S., Nelken, S., Shuda, M., and Kaji, A. (1998) *Embo J 17*, 1141-51.
5. Janosi, L., Ricker, R., and Kaji, A. (1996) *Biochimie 78*, 959-69.
6. Pavlov, M. Y., Freistroffer, D. V., MacDougall, J., Buckingham, R. H., and Ehrenberg, M. (1997) *Embo J 16*, 4134-41.
7. Pavlov, M. Y., Freistroffer, D. V., Heurgue-Hamard, V., Buckingham, R. H., and Ehrenberg, M. (1997) *J Mol Biol 273*, 389-401.
8. Karimi, R., Pavlov, M. Y., Buckingham, R. H., and Ehrenberg, M. (1999) *Mol Cell 3*, 601-9.
9. Ogawa, K., and Kaji, A. (1975) *Eur J Biochem 58*, 411-9.
10. Hirashima, A., and Kaji, A. (1972) *J Mol Biol 65*, 43-58.
11. Grentzmann, G., Kelly, P. J., Laalami, S., Shuda, M., Firpo, M. A., Cenatiempo, Y., and Kaji, A. (1998) *Rna 4*, 973-83.
12. Inokuchi, Y., Hirashima, A., Sekine, Y., Janosi, L., and Kaji, A. (2000) *Embo J 19*, 3788-98.
13. Fraser, C. M., Gocayne, J. D., White, O., Adams, M. D., Clayton, R. A., Fleischmann, R. D., Bult, C. J., Kerlavage, A. R., Sutton, G., Kelley, J. M., and et al. (1995) *Science 270*, 397-403.
14. Rolland, N., Janosi, L., Block, M. A., Shuda, M., Teyssier, E., Miege, C., Cheniclet, C., Carde, J. P., Kaji, A., and Joyard, J. (1999) *Proc Natl Acad Sci U S A 96*, 5464-9.
15. Selmer, M., Al-Karadaghi, S., Hirokawa, G., Kaji, A., and Liljas, A. (1999) *Science 286*, 2349-52.
16. Kim, K. K., Min, K., and Suh, S. W. (2000) *Embo J 19*, 2362-70.
17. Toyoda, T., Tin, O. F., Ito, K., Fujiwara, T., Kumasaka, T., Yamamoto, M., Garber, M. B., and Nakamura, Y. (2000) *Rna 6*, 1432-44.
18. Lancaster, L., Kiel, M. C., Kaji, A., and Noller, H. F. (2002) *Cell 111*, 129-40.
19. Nakano, H., Yoshida, T., Uchiyama, S., Kawachi, M., Matsuo, H., Kato, T., Ohshima, A., Yamaichi, Y., Honda, T., Kato, H., Yamagata, Y., Ohkubo, T., and Kobayashi, Y. (2003) *J Biol Chem 278*, 3427-36.
20. Lee, K. M., Androphy, E. J., and Baleja, J. D. (1995) *J Biomol NMR 5*, 93-6.
21. Piotto, M., Saudek, V., and Sklenar, V. (1992) *J Biomol NMR 2*, 661-5.
22. Kay, L. E., Keifer, P., and Saarinen, T. (1992) *J Am Chem Soc 114*, 10663-10665.
23. Wishart, D. S., Bigam, C. G., Yao, J., Abildgaard, F., Dyson, H. J., Oldfield, E., Markley, J. L., and Sykes, B. D. (1995) *J Biomol NMR 6*, 135-40.
24. Bax, A., Vuister, G. W., Grzesiek, S., Delaglio, F., Wang, A. C., Tschudin, R., and Zhu, G. (1994) *Methods Enzymol 239*, 79-105.
25. Kay, L. E. (1995) *Prog Biophys Mol Biol 63*, 277-99.
26. Delaglio, F., Grzesiek, S., Vuister, G. W., Zhu, G., Pfeifer, J., and Bax, A. (1995) *J Biomol NMR 6*, 277-93.
27. Garrett, D. S., Powers, R., Gronenborn, A. M., and Clore, G. M. (1991) *J Magn Reson 95*, 214-220.
28. Spera, S., and Bax, A. (1991) *J Am Chem Soc 113*, 5490-5492.

29. Cate, J. H., Yusupov, M. M., Yusupova, G. Z., Earnest, T. N., and Noller, H. F. (1999) *Science 285*, 2095-104.
30. Ban, N., Nissen, P., Hansen, J., Capel, M., Moore, P. B., and Steitz, T. A. (1999) *Nature 400*, 841-7.
31. Clemons, W. M., Jr., May, J. L., Wimberly, B. T., McCutcheon, J. P., Capel, M. S., and Ramakrishnan, V. (1999) *Nature 400*, 833-40.
32. Ban, N., Nissen, P., Hansen, J., Moore, P. B., and Steitz, T. A. (2000) *Science 289*, 905-20.
33. Schluenzen, F., Tocilj, A., Zarivach, R., Harms, J., Gluehmann, M., Janell, D., Bashan, A., Bartels, H., Agmon, I., Franceschi, F., and Yonath, A. (2000) *Cell 102*, 615-23.
34. Wimberly, B. T., Brodersen, D. E., Clemons, W. M., Jr., Morgan-Warren, R. J., Carter, A. P., Vonrhein, C., Hartsch, T., and Ramakrishnan, V. (2000) *Nature 407*, 327-39.
35. Sette, M., van Tilborg, P., Spurio, R., Kaptein, R., Paci, M., Gualerzi, C. O., and Boelens, R. (1997) *Embo J 16*, 1436-43.
36. Czworkowski, J., Wang, J., Steitz, T. A., and Moore, P. B. (1994) *Embo J 13*, 3661-8.
37. Wang, Y., Jiang, Y., Meyering-Voss, M., Sprinzl, M., and Sigler, P. B. (1997) *Nat Struct Biol 4*, 650-6.
38. Song, H., Mugnier, P., Das, A. K., Webb, H. M., Evans, D. R., Tuite, M. F., Hemmings, B. A., and Barford, D. (2000) *Cell 100*, 311-21.
39. Grzesiek, S., and Bax, A. (1993) *J Am Chem Soc 115*, 12593-12594.
40. Press, W. H., Teukolsky, S. A., Vettring, W. T., and Flannery, B. P. (1992) *Numerical Recipes*, Cambridge University Press, Cambridge, U.K.
41. Davis, D. G., Perlman, M. E., and London, R. E. (1994) *J Magn Reson B104*, 266-275.
42. Powers, R., Garrett, D. S., March, C. J., Frieden, E. A., Gronenborn, A. M., and Clore, G. M. (1993) *Biochemistry 32*, 6744-62.
43. Nilges, M. (1993) *Proteins 17*, 297-309.
44. Wuthrich, K. (1986) *NMR of Proteins and Nucleic Acids*, Wiley, New York.
45. Clore, G. M., and Gronenborn, A. M. (1991) *Science 252*, 1390-9.
46. Cornilescu, G., Delaglio, F., and Bax, A. (1999) *J Biomol NMR 13*, 289-302.
47. Hu, J. S., and Bax, A. (1997) *J Biomol NMR 9*, 323-8.
48. Hu, J. S., Grzesiek, S., and Bax, A. (1997) *J Am Chem Soc 119*, 1803-1804.
49. Clore, G. M., Gronenborn, A. M., Szabo, A., and Tjandra, N. (1998) *J Am Chem Soc 120*, 4889-4890.
50. Brunger, A. T., Adams, P. D., Clore, G. M., DeLano, W. L., Gros, P., Grosse-Kunstleve, R. W., Jiang, J. S., Kuszewski, J., Nilges, M., Pannu, N. S., Read, R. J., Rice, L. M., Simonson, T., and Warren, G. L. (1998) *Acta Crystallogr D Biol Crystallogr 54 (Pt 5)*, 905-21.
51. Stein, E. G., Rice, L. M., and Brunger, A. T. (1997) *J Magn Reson 124*, 154-164.
52. Koradi, R., Billeter, M., and Wuthrich, K. (1996) *J Mol Graph 14*, 51-5, 29-32.
53. Laskowski, R. A., MacArthur, M. W., Moss, D. S., and Thornton, J. M. (1993) *J Appl Crystallogr 26*, 283-291.
54. Neri, D., Szyperski, T., Otting, G., Senn, H., and Wuthrich, K. (1989) *Biochemistry 28*, 7510-6.
55. Tjandra, N., Feller, S. E., Pastor, R. W., and Bax, A. (1995) *J Am Chem Soc 117*, 12562-12566.
56. Kashimori, H., Yoshida, T., Kijima, H., Shimahara, H., Uchiyama, S., Ishino, T., Shuda, M., Nakano, H., Shibata, Y., Saihara, Y., Ohkubo, T., Kaji, A., and Kobayashi, Y. (1999) *J Biomol NMR 15*, 341-2.

57. Argos, P. (1988) *Protein Eng 2*, 101-13.
58. Tjandra, N., Garrett, D. S., Gronenborn, A. M., Bax, A., and Clore, G. M. (1997) *Nat Struct Biol 4*, 443-9.
59. Tjandra, N., and Bax, A. (1997) *Science 278*, 1111-4.
60. Atarashi, K., and Kaji, A. (2000) *J Bacteriol 182*, 6154-60.
61. Ohnishi, M., Janosi, L., Shuda, M., Matsumoto, H., Hayashi, T., Terawaki, Y., and Kaji, A. (1999) *J Bacteriol 181*, 1281-91.
62. Fujiwara, T., Ito, K., Nakayashiki, T., and Nakamura, Y. (1999) *FEBS Lett 447*, 297-302.
63. Lupas, A. (1996) *Trends Biochem Sci 21*, 375-82.
64. Fauchere, J. L., and Pliska, V. (1983) *Eur J Med Chem 18*, 369-375.
65. Xiao, L., and Honig, B. (1999) *J Mol Biol 289*, 1435-44.
66. Jaenicke, R., and Bohm, G. (1998) *Curr Opin Struct Biol 8*, 738-48.
67. Janosi, L., Mori, H., Sekine, Y., Abragan, J., Janosi, R., Hirokawa, G., and Kaji, A. (2000) *J Mol Biol 295*, 815-29.
68. Feher, V. A., and Cavanagh, J. (1999) *Nature 400*, 289-93.
69. Ishima, R., Freedberg, D. I., Wang, Y. X., Louis, J. M., and Torchia, D. A. (1999) *Structure Fold Des 7*, 1047-55.
70. Berendsen, H. J. C., van der Spoel, D., and van Drunen, R. (1995) *Comp Phys Comm 91*, 43-65.
71. Lindahl, E., Hess, B., and van der Spoel, D. (2001) *J Mol Mod 7*, 306-317.
72. Berendsen, H. J. C., Postma, J. P. M., van Gunsteren, W. F., and Harmans, J. (1981) in *Intermolecular Forces* (Pullman, B., Ed.) pp 331-342, Reidel, Dordrecht.
73. Darden, T., York, D., and Pedersen, L. (1993) *J Chem Phys 98*, 10089-10092.
74. Hess, B., Bekker, H., Berendsen, H. L. C., and Fraaije, J. G. E. M. (1997) *J Comp Chem 18*, 1463-1472.
75. Berendsen, H. J. C., Postma, J. P. M., DiNola, A., and Haak, J. R. (1984) *J Chem Phys 81*, 3684-3690.
76. Nakano, H., Uchiyama, S., Yoshida, T., Ohkubo, T., Kato, H., Yamagata, Y., and Kobayashi, Y. (2002) *Acta Crystallogr D Biol Crystallogr 58*, 124-6.
77. Amadei, A., Linssen, A. B., and Berendsen, H. J. (1993) *Proteins 17*, 412-25.
78. Lipari, G., and Szabo, A. (1982) *J Am Chem Soc 104*, 4546-4559.
79. Lipari, G., and Szabo, A. (1982) *J Am Chem Soc 104*, 4559-4570.
80. Peng, J. W., Thanabal, V., and Wagner, G. (1991) *J Magn Reson 95*, 421-427.
81. Kay, L. E., Nicholson, L. K., Delaglio, F., Bax, A., and Torchia, D. (1992) *J Magn Reson 97*, 359-375.
82. Yoshida, T., Kijima, H., Oka, S., Uchiyama, S., Nakano, H., Ohkubo, T., and Kobayashi, Y. (2002) *J Biomol NMR 22*, 195-196.
83. Tjandra, N., Wingfield, P., Stahl, S., and Bax, A. (1996) *J Biomol NMR 8*, 273-84.
84. Abragam, A. (1961) *The principles of Nuclear Magnetic Resonance*, Clarendon Press, Oxford.
85. Kroenke, C. D., Rance, M., and Palmer, A. G. (1999) *J Am Chem Soc 121*, 10119-10125.
86. Mandel, A. M., Akke, M., and Palmer, A. G., 3rd. (1995) *J Mol Biol 246*, 144-63.
87. Clore, G. M., Szabo, A., Bax, A., Kay, L. E., Driscoll, P. C., and Gronenborn, A. M. (1990) *J Am Chem Soc 112*, 4989-4991.
88. Baber, J. L., Szabo, A., and Tjandra, N. (2001) *J Am Chem Soc 123*, 3953-3959.
89. Braddock, D. T., Louis, J. M., Baber, J. L., Levens, D., and Clore, G. M. (2002) *Nature 415*, 1051-6.

90. Komeiji, Y., Uebayasi, M., and Yamato, I. (1994) *Proteins 20*, 248-58.
91. Yoshida, T., Uchiyama, S., Nakano, H., Kashimori, H., Kijima, H., Ohshima, T., Saihara, Y., Ishino, T., Shimahara, H., Yokose, K., Ohkubo, T., Kaji, A., and Kobayashi, Y. (2001) *Biochemistry 40*, 2387-96.
92. Philippopoulos, M., Mandel, A. M., Palmer, A. G., 3rd, and Lim, C. (1997) *Proteins 28*, 481-93.
93. Shuker, S. B., Hajduk, P. J., Meadows, R. P., and Fesik, S. W. (1996) *Science 274*, 1531-4.
94. Rao, A. R., and Varshney, U. (2002) *Microbiology 148*, 3913-20.
95. Ito, K., Fujiwara, T., Toyoda, T., and Nakamura, Y. (2002) *Mol Cell 9*, 1263-72.
96. Joseph, S., and Noller, H. F. (1998) *Embo J 17*, 3478-83.
97. Hirokawa, G., Kiel, M. C., Muto, A., Selmer, M., Raj, V. S., Liljas, A., Igarashi, K., Kaji, H., and Kaji, A. (2002) *Embo J 21*, 2272-81.

Acknowledgements

The studies presented here have been performed under the direction of Professor Yuji Kobayashi, Graduate School of Pharmaceutical Sciences, Osaka University. The author would like to express his deepest gratitude to Prof. Y. Kobayashi for his cordial guidance, giving me best experimental environment, and profitable discussion.

The author wishes to express his sincere thanks to Associate Professor Tadayasu Ohkubo, Graduate School of Pharmaceutical Sciences, Osaka University, for his helpful criticism and encouragement. The author also wishes to thank Dr. Susumu Uchiyama and Dr Hiroaki Nakano for fruitful discussions and advices. Thanks are also due to Professor Motomasa Kobayashi, Tatsuya Takagi and Takeshi Imanishi for reading the draft and making a number of helpful suggestions.

The author wishes to express his cordial appreciation to Hiromasa Kashimori, Hiroyuki Kijima, Tamiko Ohsima, Shinichiro Oka, Tadayuki Kawasaki and all the member of Laboratory of Biophysical Chemistry, Graduate School of Pharmaceutical Sciences, Osaka University, for a number of helpful comments and experimental supports.

I thank my family and friends for their understanding and supports during the course of this work.